BBA - Molecular and Cell Biology of Lipids 1864 (2019) 1017–1030

Contents lists available at ScienceDirect

BBA - Molecular and Cell Biology of Lipids

journal homepage: www.elsevier.com/locate/bbalip

Saturated fatty acids induce NLRP3 activation in human macrophages through K^+ efflux resulting from phospholipid saturation and Na, K-ATPase disruption

Marco A. Gianfrancesco[a,b], Jonas Dehairs[c], Laurent L'homme[d], Gaëtan Herinckx[e], Nathalie Esser[a,b], Olivia Jansen[f], Yvette Habraken[g], Cédric Lassence[g], Johan V. Swinnen[c], Mark H. Rider[e], Jacques Piette[g], Nicolas Paquot[a,b], Sylvie Legrand-Poels[a,*]

[a] Laboratory of Immunometabolism and Nutrition, GIGA-Inflammation, Infection & Immunity, University of Liège, Liège, Belgium
[b] Division of Diabetes, Nutrition and Metabolic Disorders, Department of Medicine, University Hospital of Liège, Liège, Belgium
[c] Laboratory of Lipid Metabolism and Cancer, Department of Oncology, KU Leuven, Leuven, Belgium
[d] University of Lille, Inserm, University Hospital of Lille, Pasteur Institute of Lille, U1011 - EGID, F-59000 Lille, France
[e] de Duve Institute, Catholic University of Louvain, 1200 Brussels, Belgium
[f] Laboratory of Pharmacognosy, CIRM, University of Liège, Liège, Belgium
[g] Laboratory of Virology and Immunology, GIGA-Molecular Biology of Diseases, University of Liège, Liège, Belgium

ARTICLE INFO

Keywords:
NLRP3 inflammasome
Obesity
Free fatty acids
Phospholipid
Na
K-ATPase
K^+ efflux

ABSTRACT

NLRP3 inflammasome plays a key role in Western diet–induced systemic inflammation and was recently shown to mediate long-lasting trained immunity in myeloid cells. Saturated fatty acids (SFAs) are sterile triggers able to induce the assembly of the NLRP3 inflammasome in macrophages, leading to IL-1β secretion while unsaturated ones (UFAs) prevent SFAs-mediated NLRP3 activation. Unlike previous studies using LPS-primed bone marrow derived macrophages, we do not see any ROS or IRE-1α involvement in SFAs-mediated NLRP3 activation in human monocytes-derived macrophages. Rather we show that SFAs need to enter the cells and to be activated into acyl-CoA to lead to NLRP3 activation in human macrophages. However, their β-oxidation is dispensable. Instead, they are channeled towards phospholipids but redirected towards lipid droplets containing triacylglycerol in the presence of UFAs. Lipidomic analyses and Laurdan fluorescence experiments demonstrate that SFAs induce a dramatic saturation of phosphatidylcholine (PC) correlated with a loss of membrane fluidity, both events inhibited by UFAs. The silencing of CCTα, the key enzyme in PC synthesis, prevents SFA-mediated NLRP3 activation, demonstrating the essential role of the *de novo* PC synthesis. This SFA-induced membrane remodeling promotes a disruption of the plasma membrane Na, K-ATPase, instigating a K^+ efflux essential and sufficient for NLRP3 activation. This work opens novel therapeutic avenues to interfere with Western diet-associated diseases such as those targeting the glycerolipid pathway.

Abbreviations: ACS, acylCoA synthetase; ACSLs, long-chain fatty acyl CoA synthetases; AMPK, AMP-activated protein kinase; ASC, apoptosis-associated speck-like protein; ATF4, activating transcription factor 4; ATMs, adipose tissue macrophages; BMDCs, bone-marrow-derived dendritic cells; BMDMs, bone-marrow-derived macrophages; BSA, Bovine Serum Albumin; C16:0, palmitate; C18:0, stearate; C18:1, oleate; C18:2, linoleate; CCTα, CTP-phosphocholine-cytidyl transferase alpha; CPT, carnitine palmitoyltransferase; DAG, diacylglycerol; DAMPs, danger associated molecular patterns; DGAT1, diacylglycerol O-acyltransferase 1; ER, endoplasmic reticulum; FFAR1–4, free fatty acid receptor 1–4; FFAs, free fatty acids; GP, Generalized Polarization; HFD, high fat diet; HPRT1, Hypoxanthine Phosphoribosyltransferase 1; IRE1α, inositol-requiring enzyme 1-alpha; Ld, liquid disordered; LD, lipid droplets; Lo, liquid ordered; LPS, Lipopolysaccharide; LRR, leucine-rich repeat; MDMs, monocytes-derived macrophages; mROS, mitochondrial reactive oxygen species; NEK7, NIMA Related Kinase 7; NF-κB, Nuclear Factor-κB; NLR, nucleotide-binding oligomerization domain (NOD)-, leucine-rich repeat (LRR); NLRP3, nucleotide-binding domain, leucine-rich-containing family, pyrin domain-containing-3; NOD, nucleotide-binding oligomerization domain; PAMPs, pathogen associated molecular patterns; PBMCs, peripheral blood mononuclear cells; PC, phosphatidylcholine; PE, phosphatidylethanolamine; PERK, PKR-like ER kinase; PI, phosphatidylinositol; PMA, phorbol 12-myristate 13-acetate; PS, phosphatidylserine; SEM, Standard Error of the Mean; SERCA, sarco/endoplasmic reticulum Ca^{2+} ATPase; SFAs, saturated fatty acids; So, solid ordered; T2D, type 2 diabetes; TAG, triacylglycerol; TC, Triacsin C; TLC, thin layer chromatography; TLR, Toll-like Receptor; TNFα, tumor necrosis factor-alpha; UFAs, unsaturated fatty acids; UPR, Unfolded Protein Response; WD, Western diet; Xbp1s, spliced X-Box Binding Protein 1

* Corresponding author.
E-mail address: s.legrand@uliege.be (S. Legrand-Poels).

https://doi.org/10.1016/j.bbalip.2019.04.001
Received 23 February 2018; Received in revised form 20 December 2018; Accepted 6 January 2019
Available online 04 April 2019
1388-1981/ © 2019 Elsevier B.V. All rights reserved.

1. Introduction

Obesity has become a major health burden in developed countries. It promotes insulin resistance and is strongly associated with metabolic defects such as hyperglycemia, dyslipidemia and hypertension, which together are termed "metabolic syndrome" [1]. These disorders contribute to higher rates of morbidity and mortality due to the increased risk of developing type 2 diabetes (T2D), non-alcoholic fatty liver disease, cardiovascular diseases and cancer [2]. Moreover, a chronic low-grade inflammation has been observed in abdominal obesity that plays a role in the pathogenesis of obesity-related metabolic disorders [3]. This systemic inflammation results mainly from an excessive accumulation of pro-inflammatory macrophages in adipose tissue [3]. A current theory supports that weight gain and adipocytes hypertrophy induce chemokines-promoted recruitment of circulating monocytes [3]. These monocytes differentiate into macrophages secreting pro-inflammatory cytokines such as TNFα, IL-6 and IL-1β.

IL-1β has been shown to be a key contributor to the pathogenesis of T2D mainly by interfering with insulin signaling [4] and playing a critical role in the pathological deterioration of pancreatic β-cell function [5]. IL-1β production is tightly controlled and depends on two signals. First, a pro-inflammatory priming signal stimulates the transcription of *IL1β* gene through NF-κB (Nuclear Factor-κB)-dependent pathway leading to the synthesis of the Pro-IL-1β. Secondly, the Pro-IL-1β cleavage in its biologically active form is mainly mediated by a large cytosolic multiprotein platform termed "inflammasome" [6,7]. Inflammasomes are usually formed through the interaction between a member of the NLR family (nucleotide-binding oligomerization domain (NOD)-, leucine-rich repeat (LRR)-containing proteins), an adaptor protein ASC (apoptosis-associated speck-like protein containing a Caspase recruitment domain) and the Pro-caspase-1. Their assembly is triggered in response to pathogen- and danger-associated molecular patterns (PAMPs and DAMPs) [6,7]. Proximity-induced pro-caspase 1 autoprocessing results in the formation of active caspase-1, which, in turn, can cleave the Pro-IL-1β and lead to the release of IL-1β.

The NLRP3 (nucleotide-binding domain, leucine-rich-containing family, pyrin domain-containing-3) inflammasome is characterized by the sensing of a large array of DAMPs such as extracellular ATP, pore-forming toxins and various crystalline and particulate matter (Alum, cholesterol, monosodium urate, silica, asbestos) [8]. More recently, NLRP3 was also shown to respond to metabolic danger signals that accumulate during obesity like glucose, ceramide and free fatty acids (FFAs) [9,10]. Thanks to the Nlrp3$^{-/-}$ high fat diet (HFD) mouse model, NLRP3 inflammasome has been shown to instigate obesity-induced inflammation and insulin resistance (IR) [11,12]. Our group also highlighted the role of NLRP3 inflammasome in obesity-linked metabolic syndrome by demonstrating caspase-1 activation in visceral adipose tissue macrophages (ATMs) in metabolically unhealthy compared to metabolically healthy obese patients [13].

Due to the very large range of divergent NLRP3 triggers, it is unlikely that NLRP3 directly recognizes its agonists. It is usually accepted that NLRP3 rather senses cell homeostasis disruption. Several mechanisms have been proposed to account for NLRP3 activation including K^+ efflux, lysosomal destabilization induced by various crystals, reactive oxygen species (ROS) production, mitochondria dysfunction and Ca^{2+} homeostasis disruption [8,14]. However, K^+ efflux seems to be a common denominator to many NLRP3 activators even if its origin can vary according to the NLRP3 trigger [15–17]. More recently, NLRP3 aggregation on the dispersed trans-Golgi network (dTGN) through phosphatidylinositol-4-phosphate (PtdIns4P) binding has been shown as a common cellular signal essential for the inflammasome activation by diverse stimuli [18]. K^+ efflux helps the NLRP3 recruitment to dTGN *via* ionic bonding between negatively charged PtdIns4P on dTGN membranes and the positively charged polybasic region of NLRP3 [18]. K^+ efflux is also needed for NLRP3 interaction with NEK7 (NIMA Related Kinase 7), a Ser/Thr kinase specifically required for NLRP3 activation [17,19].

The important contribution of the NLRP3 inflammasome in the pathogenesis of obesity-linked IR and T2D prompted several groups to study the mechanisms underlying FFA-mediated NLRP3 inflammasome activation [11,12]. Previous studies have demonstrated the inhibition of AMP-activated protein kinase (AMPK) by palmitate (C16:0) in LPS-primed bone-marrow-derived macrophages (BMDMs), followed by the defective autophagy and the accumulation of mitochondrial reactive oxygen species (mROS) resulting probably from an impairment of mitophagy [12]. More recently, palmitate and stearate (C18:0) have been proposed to mediate NLRP3 inflammasome activation in LPS-primed BMDCs (bone-marrow-derived dendritic cells) or BMDMs through the activation of IRE1α (inositol-requiring enzyme 1-alpha), one of the three ER stress sensors [20]. According to these authors, saturated fatty acids (SFAs)-induced IRE1α activation does not depend on the sensing of unfolded proteins but does occur in response to the accumulation of saturated phosphatidylcholine (PC) [20]. Our group demonstrated the activation of NLRP3 inflammasome by SFAs and its inhibition by the co-treatment with unsaturated fatty acids (UFAs) in human monocytes-derived macrophages (MDMs) and PMA (phorbol 12-myristate 13-acetate)-differentiated THP-1 cells [21]. Since neither ROS, nor IRE1α seem to be required for SFAs-mediated NLRP3 activation in any of both human macrophages models, we further explored underlying mechanisms. In the present study, we demonstrate that SFAs-mediated NLRP3 inflammasome activation involves a K^+ efflux resulting from Na^+, K^+-ATPase disruption due to the accumulation of saturated PC and loss of plasma membrane fluidity. All these events are reversed by co-treatment with UFAs.

2. Material and methods

2.1. Preparation of FFA solutions

Following products were obtained from Sigma-Aldrich: low endotoxin BSA, palmitic acid, stearic acid, oleic acid and linoleic acid (#A8806, #P0500, #S4751, #O1008, #L1376, respectively). The FFA solutions were prepared and stored as previously described [21].

2.2. Cell culture and treatment

THP-1 cell line (ATCC, authentified by DSMZ, Germany, 2011) was cultured at 37 °C under 5% CO_2 atmosphere and below 1.0×10^6 cells/ml in RPMI 1640 with glutamine and 10% heat-inactivated FBS, 100 U/ml penicillin and 100 U/ml streptomycin (Lonza). THP-1 cells were differentiated with 100 ng/ml of PMA (Sigma) for 24 h, rinsed with PBS and maintained overnight in renewed medium before treatments. After informed consent, healthy donors allowed us to obtain buffy coats (Red Cross, Belgium). Density gradient centrifugation with Ficoll-Paque PLUS (GE Healthcare) was performed from buffy coats to obtain human peripheral blood mononuclear cells (PBMCs). CD14 MicroBeads (Miltenyi Biotec) were used to isolate primary monocytes from PBMCs according to the manufacturer's instructions. Trials were permitted by the ethical committee of the University of Liege. The isolated monocytes were differentiated in RPMI 1640 with 20% FBS and 100 ng/ml of human M-CSF premium grade (Miltenyi Biotec) for seven days to obtain monocyte-derived macrophages (MDMs). After differentiation, cells were treated with following compounds as indicated in figure captions: FFAs, Triascin C (Santa Cruz, # sc-200574), STF-083010 (Med Chem Express # HY-15845), trans-ISRIB (Cayman chemicals, # 16258), ouabain octahydrate (Sigma, # O3125), nigericin (Enzo life science, # BML-CA421), antimycin A from *Streptomyces* sp. (Sigma, # A8674), etomoxir (Sigma, # E1905), Alum (Thermo Fisher Scientific, #77161), H_2O_2 (Sigma, # H1009), 4μ8C (Axon Medchem, # Axon 1902) and MitoTEMPO (Enzo life science, # ALX-430-150).

2.3. Measurement of cellular and mitochondrial ROS

In PMA-differentiated THP-1 cells, cellular and mitochondrial ROS production was detected with H2DCFDA (Invitrogen™, # C6827) and MitoSOX (Invitrogen™, # M36008), respectively. For measurement of cellular ROS, cells were pre-incubated with H2DCFDA (5 μM, 30 min) and treated as indicated in figure legends. For measurement of mitochondrial ROS, cells were treated as indicated in figure legends followed by 30 min of incubation with MitoSOX. Fluorescence corresponding to cellular and mitochondrial ROS production was measured through EnSpire 2300 Multilabel Reader according to the manufacturer's recommendations. In MDMs, mitochondrial ROS were detected with MitoSOX (5 μM). Cells were pre-incubated with MitoSOX (5 μM, 30 min) at 37 °C before being washed in warm culture medium and treated as indicated in figure legends. At the end of incubation period, cells were subjected to flow cytometric analysis (BD Canto II) using the Phycoerythrin (PE) channel.

2.4. Radiolabeled stearate flux into lipids

PMA-differentiated THP-1 cells were cultured in 6 well plates and treated with 200 μM of stearic acid and 2 μCi/ml of radiolabeled [1-14C] stearic acid in the presence or absence of 200 μM of oleate for 8 h. After washing of the cells with ice-cold PBS, total lipids were extracted with chloroform/methanol (2:1), followed by 10 min vortexing and centrifugation at 1000 × *g* for 10 min. Supernatants containing total lipids were evaporated overnight. Dried lipids were resuspended in chloroform/methanol (2:1) and analyzed by thin-layer chromatography (TLC) on TLC Silica gel 60 F254 plates (Merck), using the solvent system petroleum ether (b.p. 40–60 °C)/diethylether/formic acid (70:30:1.5). Typhoon 9400TM (Amersham Biosciences) was used to scan storage phosphor screens that have been exposed to the radioactive TLC for 4 h. The resulting digital image allows for quantitation using ImageQuant™ TL v7.0 (GE Healthcare). Lipid fractions were also visualized by anisaldehyde staining. Raw Colza extract and cholesterol were used as the lipid reference substances for lipid species identification.

2.5. Stearate uptake

PMA-differentiated THP-1 cells were cultured in 6 well plates and treated with 200 μM of stearic acid and 0.1 μCi/ml of radiolabeled [1-14C] stearic acid in the presence or absence of 200 μM of oleate. After treatments, cells were extensively rinsed with cold PBS and lysed with 50 mM NaOH before radioactivity counting with liquid scintillation analyzer (Packard, Tri-carb 1600TR).

2.6. Lipidomic analysis

Lipidomic analyses were performed as described previously [22]. Briefly, lipids were extracted from 700 μL of homogenized cells with 800 μL CH_3OH:HCl 8:1 (v/v) and 900 μL $CHCl_3$. The antioxidant 2,6-di-tert-butyl-4-methylphenol was added to the extract at a concentration of 200 μg/ml (BHT; Sigma Aldrich). The organic phase was evaporated at room temperature using a Savant Speedvac (Thermo Fisher Scientific) and the resulting lipid pellet was stored under argon at −20 °C. Prior to analysis, lipid pellets were dissolved in running solution (NH_4OH:$CHCl_3$:CH_3OH; 1.25:10:90; v/v/v). Lipid standards PS25:0, PS31:1, PS37:4, PI25:0, PI43:6, PE25:0, PE43:6, PC25:0, PC43:6, were purchased from Avanti Polar Lipids and were added to the sample in ratio to the DNA concentration of the original homogenized sample. The phospholipids were analyzed by electrospray ionization tandem mass spectrometry (ESI-MS/MS) on 4000 QTRAP system (AB SCIEX) using a robotic nanosource for sample injection (TriVersa NanoMate: Advion Biosciences). Phospholipid profiling was performed by precursor ion or neutral loss scanning at a collision energy of −60 eV, −35 eV, 35 eV, 50 eV/45 eV, for precursor 241 (phosphatidylinositol, PI), neutral loss 87 (phosphatidylserine, PS), neutral loss 141 (phosphatidylethanolamine, PE) and precursor 184 (phosphatidylcholine, PC) respectively. Quantification was done with multiple reaction monitoring with a signal averaging period of 3 min. Measurements were corrected for hydrogen, nitrogen, carbon and oxygen isotope effects using the algorithm described by [22]. Only species with a signal intensity above 5 times the blank were reported. Each lipid species is represented as a % of the total lipid content of a specific class.

2.7. Subcellular fractionation

5×10^6 cells were transferred into 250 μl of fractionation buffer (20 mM HEPES pH 7.4, 10 mM KCl, 2 mM $MgCl_2$, 1 mM EDTA, 1 mM EGTA, 1 mM DTT and complete protease inhibitor cocktail (Roche Applied Science)) by scraping and left on ice 15 min. Cell suspension was passed through a 25 gauge needle until cells were lysed and left on ice 20 min. Samples were centrifuged at 720 × *g* for 5 min. Nuclear pellet was discarded and the cytoplasm, membrane and mitochondria containing supernatant was centrifuged at 8000 × *g* for 5 min. Mitochondria containing pellet was discarded and the cytoplasm and membrane containing supernatant was ultracentrifuged at 100,000 × *g* for 1 h. Cytoplasm containing supernatant was stored at −20 °C before protein dosage and immunoblotting. Membrane containing pellet was washed by adding 200 μl of fractionation buffer and passed through a 25 gauge needle several times before being ultracentrifuged at 100,000 × *g* for 45 min. The membrane pellet was resuspended in 50 μl of TBS with 0.1% SDS and sonicated for 5 min before protein dosage and immunoblotting. All centrifugations were done at 4 °C and samples were kept on ice throughout the procedure.

2.8. Immunoblot analysis

Total extracts were prepared by scraping the cells in total lysis buffer (160 μl/2 × 10^6 cells) [87.5 mM Tris-HCl pH 7.5, 75 mM NaCl, 0.5 mM EDTA, 0.5% Igepal, 0.125% sodium deoxycholate, 2% SDS, 10% glycerol, 3% β-mercaptoethanol, 0.002% bromophenol blue, 0.5 mM PMSF, and complete protease inhibitor cocktail (Roche Applied Science)]. Samples were stored at −20 °C after passing them several times through a 25-gauge needle. Culture supernatants were stored at −80 °C after a centrifugation to eliminate cells debris. Total lysates (30 μl) or supernatants (18 μl) were subjected to SDS-PAGE. After migration, proteins were transferred to a PVDF membrane. Primary antibodies used are the following ones: anti-IL-1beta propeptide (R&D Systems, #MAB6964), anti-IL-1 beta (R&D Systems, #AF-201-NA), anti-HSP90 (Santa Cruz, #sc-7947), anti-αtubulin (Sigma, #T6199), anti-Na, K-ATPase α1 subunit (Abcam, #ab76020), anti-CCTα (Cell signaling, #6931S) and anti-ATF4 (Cell signaling, #11815). HRP conjugated secondary antibodies are anti-rabbit (Dako, #P0217), anti-goat (Dako, #P0160), and anti-mouse (Dako, #P0447). ECL or ECL plus Western blotting substrate (Pierce) and the digital imaging system ImageQuant LAS 4000 (GE Healthcare) were used to detect HRP enzyme activity.

2.9. siRNAs transfection

THP-1 cells (0.25 × 10^6) were plated in a 24-well plate and differentiated with 100 ng/ml of PMA (Sigma) for 24 h, rinsed with PBS and maintained overnight in renewed medium. Transfection complexes were prepared in RPMI1640 by adding 3 μl of HiPerFect transfection reagent (Qiagen), and 400 nM of short interfering RNAs (siRNAs) in a final volume of 100 μl and were added to PMA-differentiated THP-1 cells. After 6 h, 600 μl of supplemented medium were added. 72 h after transfection, PMA-differentiated THP-1 cells were rinsed with PBS and stimulated as described in the figure legends. The siRNAs were from IDT: siPCYT1A #1-Fw: 5′-GUCAGCUUUAUCAACGAGAAGAAAT-3′;

siPCYT1A#1-Rv: 5′-AUUUCUUCUCGU UGAUAAAGCUGACAU-3′, siPCYT1A#2-Fw: 5′-GCUCUCUGUUGAAUUCCAAAUUG TG-3′; siPCYT1A#2-Rv: 5′-CACAAUUUGGAAUUCAACAGAGAGCUU-3′. Non-targeting or scrambled siRNAs (IDT) were used as negative control.

2.10. Propargylcholine incorporation assay

De novo synthesis of PC was quantified using Propargylcholine and click-chemistry reaction. Propargylcholine is metabolized similarly to choline and incorporated into neo-synthetized PC. Then click chemistry reaction between the alkyne group of Propargylcholine with an azide derivative of Alexa Fluor 488 allows quantitative measurement of neo-synthetized PC. Propargylcholine (Jena Bioscience, #CLK-066, 200 μM) was added simultaneously with FFAs during 8 h. Then click-chemistry reaction was immediately performed on fixed cells (4% formaldehyde) with Alexa Fluor 488 Azide (Invitrogen, #A10266) using Click-iT Cell Reaction Buffer Kit (Invitrogen, #C10269) according to the manufacturer's instructions. Fluorescence was quantified with FilterMax F5 plate reader (Molecular Device).

2.11. ELISA

IL-1 beta Human Uncoated ELISA Kit (Thermo Scientific) was used to measure secreted IL-1β in supernatants according to the manufacturer's recommendations.

2.12. Laurdan two-photon microscopy

After the treatments, cells were washed three times with PBS and incubated with 2,5 μM Laurdan in a 5% CO_2 incubator for 1 h in the dark. Afterwards, two-photon excitation microscopy (Zeiss LSM 510 microscope) was performed at room temperature and Laurdan intensity images were obtained using a Plan-Neofluar 40×/1.3 Oil DIC objective under excitation at 780 nm with a Mai Tai Ti: Sapphire laser (Spectra-Physics). Internal photon multiplier tubes collected 8-bit, unsigned images at a scan speed of 1.6 μs/pixel. Two Laurdan intensity images were recorded simultaneously with emission in the range of 390–465 nm and 500–550 nm. The measure of membrane fluidity was obtained by using Generalized Polarization (GP) value, defined as: $GP = (I440 - I510) / (I440 + I510)$ where I440 and I510 are the emission intensities captured with the 390–465 nm and 500–550 nm filters, respectively. The GP formula was applied to each pixel using the two Laurdan intensity images and GP images were pseudo-colored in ImageJ. The colors indicate different GP values following the reported scale.

2.13. Ouabain-sensitive $^{86}Rb^+$ uptake

After treatment, the cells were incubated in medium containing $^{86}Rb^+$ (PerkinElmer, #NEZ072001MC, 5 μCi/ml) in the presence or absence of ouabain (100 μM). After 30 min, the cells were washed with PBS and lysed in 0.5%Triton X-100 containing buffer for liquid scintillation counting (Packard, Tri-carb 2100TR). Ouabain-sensitive $^{86}Rb^+$ uptake was calculated as the difference between the total $^{86}Rb^+$ uptake and $^{86}Rb^+$ uptake in presence of ouabain. Aliquots corresponding to different amounts of $^{86}Rb^+$ (pmol) were counted to construct a calibration curve for quantifying $^{86}Rb^+$ uptake (pmol) into cells.

2.14. qRT-PCR

Total RNAs were extracted with TriPure Isolation Reagent (Roche) according to the manufacturer's protocol. Extracted RNA was quantified with Nanodrop 1000 spectrophotometer (Thermo scientific) and 500 ng of RNA were reverse-transcribed to acquire cDNA (RevertAid H Minus First Strand cDNA Synthesis Kit, Thermo Scientific). Three independent experiments were quantified in triplicate by qRT-PCR performed on a LightCycler 480 (Roche Applied Science). The 2-delta delta C method was used to calculate relative gene expression with HPRT1 as housekeeping gene [23]. Used primers: HPRT1-Fw: 5′-TGACACTGGCAAAA CAATGCA-3′; HPRT1-Rv: 5′-GCTTGCGACCTTGACCATCT-3′, Xbp1s-Fw: 5′-CTGAGTCCGCAGCAGGTG-3′; Xbp1s-Rv: 5′-ACTGGGTCCAAGT TGTCC AG-3′.

2.15. Lipid droplet staining

After treatment, cells were fixed (4% paraformaldehyde, 20 min, 37 °C) and permeabilized (0.1% saponin) before staining nucleic acid with Hoechst 33258 (Thermo Fisher Scientific, #AC229891000) and lipid droplet with LipidTOX (Invitrogen™, #H34477) according to the manufacturer's recommendations. Images were acquired using a Leica SP5 confocal microscope (Leica Microsystems) using LAS-AF software. The microscope is equipped with 405 nm, Multi-Argon laser, 561 nm and 633 nm laser lines, three Photomultiplier tubes and one HyD detector. Images were scanned using 63×/1.3 glycerol objective lense (magnification/numerical aperture).

2.16. Statistical analyses

GraphPad Prism 6 for Mac OS X (GraphPad Software, Inc.) was used for statistical analyses. Analyses are described in figure captions and presented as means ± SEM. Significance is indicated by a symbol.

2.17. Heat map

Heat maps were drawn with Morpheus, a web-based tool for matrix visualization and analysis. A global color scale was applied with white set to zero. Morpheus is available on: https://software.broadinstitute.org/morpheus/.

3. Results

3.1. Neither ROS nor IRE-1α are involved in SFAs-mediated NLRP3 inflammasome activation in human macrophages

We previously demonstrated an activation of the NLRP3 inflammasome in response to SFAs in human MDMs and PMA-differentiated THP-1 cells [21]. This well-known human macrophages model expressing high levels of Pro-IL-1β and NLRP3 is very suited to study the second signal leading to NLRP3 inflammasome assembly [21]. In this model, the production of high IL-1β levels is observed after 8 h treatment with SFAs (stearate, palmitate, 200 μM) but not with UFAs (oleate (C18:1), linoleate (C18:2), 200 μM) (Fig. 1A) [21]. MDMs express low levels of the Pro-IL-1β and NLRP3 but SFA treatment (200 μM, 16 h) induces a slight NF-κB-dependent *IL1β* gene expression in addition to trigger NLRP3 inflammasome assembly leading to the secretion of low levels of IL-1β (Fig. 1B) [21]. In both kinds of human macrophages, stearate (200 μM) is more efficient than palmitate at the same concentration to induce NLRP3 activation (Fig. 1A–B).

Since ROS were initially involved in SFAs-mediated NLRP3 inflammasome assembly in LPS-primed BMDMs [12], we proceeded to ROS measurements in FFA-treated human macrophages. However, we did not detect any ROS neither in the mitochondria nor in the cytosol of PMA-differentiated THP-1 cells after treatment with SFAs (200 μM) or UFAs (200 μM) for different times when compared with vehicle alone (BSA, Bovine Serum Albumin), while mitochondrial and cytosolic ROS were measured after treatment with antimycin A and H2O2, respectively (Fig. 1C). In accordance with these observations, mitochondrial ROS were measured in antimycin A-stimulated MDMs but not in SFAs-treated MDMs (Fig. 1D).

More recently, Robblee et al. proposed a role of the UPR/IRE-1α branch in SFAs-mediated NLRP3 activation [20]. As expected, stearate induced the activation of the two UPR branches involving either IRE1

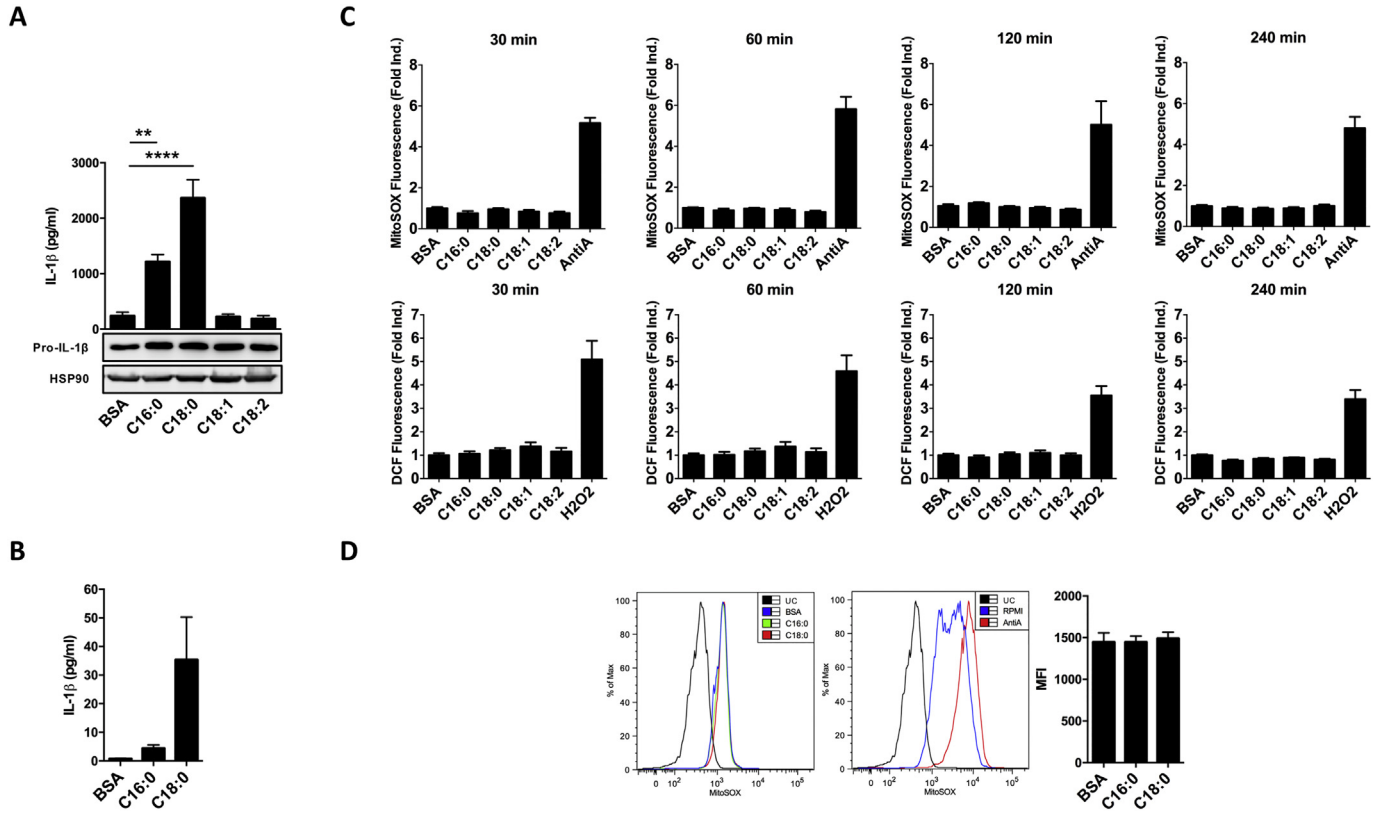


Fig. 1. ROS are not produced in human macrophages after FFAs treatments. (A) PMA-differentiated THP-1 cells were treated with BSA or FFAs (200 μM) for 8 h. IL-1β was measured in supernatants by ELISA (top). Results are presented as means ± SEM of four independent experiments. Pro-IL-1β and HSP90 levels in cytosol were determined by immunoblotting (bottom). A representative blot from minimal three independent experiments is shown. (B) MDMs were treated with BSA or FFAs (200 μM) for 16 h and IL-1β was measured in supernatants by ELISA. Results are presented as means ± SEM of three independent experiments. (C) PMA-differentiated THP-1 cells were treated with BSA, FFAs (200 μM) or antimycin A (50 μM) for the indicated times followed by 30 min of incubation with MitoSOX (5 μM) (top) or incubated with H2DCFDA (5 μM) for 30 min followed by BSA, FFAs (200 μM) or H_2O_2 treatment (1 mM) (bottom). Results are presented as means ± SEM of three independent experiments. (D) MDMs were pre-incubated with MitoSOX (5 μM, 30 min) and treated with BSA, FFAs (200 μM, 6 h) or antimycin A (50 μM, 30 min). A representative experiment is presented as fluorescence (% of Max) for the indicated treatments. Data were also quantified as fold change of median fluorescence intensity (MFI) compared with baseline and results are presented as means ± SEM of three independent experiments for FFAs. UC, unstained control. **P < 0.01; ****P < 0.0001 by one-way ANOVA followed by Dunnett's post-hoc test.

(Inositol-requiring enzyme 1-alpha) or PERK (PKR-like ER kinase), as demonstrated by the accumulation of *Xbp1s* (spliced X-Box Binding Protein 1) mRNA (Fig. 2A, B) and ATF4 (activating transcription factor 4) protein (Fig. 2G, H), respectively, in both PMA-differentiated THP-1 cells and MDMs. The inhibition of the IRE1α endoribonuclease activity by 4μ8C or STF-083010 prevented the *Xbp1* mRNA splicing as shown by the complete or partial loss of *Xbp1s* mRNA in both macrophages models (Fig. 2A, B). However, none of these inhibitors significantly affected the stearate-mediated IL-1β secretion, which rules out the contribution of the IRE1α pathway (Fig. 2C, D). ISRIB, a drug known to reverse the effects of eIF2α phosphorylation, efficiently prevented the accumulation of the ATF4 protein (Fig. 2G, H) but did not significantly down-regulate the stearate-mediated NLRP3 inflammasome activation in any kind of human macrophages (Fig. 2E, F). Altogether, these results demonstrate that neither ROS nor ER stress play a key role in the triggering of NLRP3 inflammasome assembly in response to SFA in human macrophages.

3.2. While SFAs activation into acyl-CoA is required for NLRP3 inflammasome activation, the β oxidation is dispensable for both the SFA- and UFA-mediated effects

To elucidate the mechanism by which FFAs modulate NLRP3 inflammasome assembly, we further investigated the fate of SFAs when added alone or in combination with UFAs in the extracellular medium of human macrophages. Inside cells, FFA can be activated into acyl-CoA by acylCoA synthetase (ACS) to be used in metabolic pathways like β-oxidation in mitochondria or lipid synthesis in ER [24].

In order to test whether SFAs need to be internalized into the cells and activated into acyl-CoA to induce the NLRP3 inflammasome assembly, we used Triacsin C (TC), a competitive inhibitor of ACSLs (long-chain fatty acyl CoA synthetases). While TC had no effect on IL-1β secretion in response to Alum, TC inhibited the release of IL-1β in response to palmitate and stearate without affecting the Pro-IL-1β levels in cellular extracts (Fig. 3A). To shuttle into the mitochondria and enter the β-oxidation cycle, the acyl-CoA has to be converted into acylcarnitine *via* carnitine palmitoyltransferase (CPT) 1 [10]. The inhibition of this enzyme with etomoxir did not prevent SFAs-mediated IL-1β secretion (Fig. 3B, C). Quite the opposite, preventing the palmitate mitochondrial flux by increasing etomoxir concentrations further stimulated palmitate-mediated NLRP3 inflammasome activation in a dose-dependent way (Fig. 3C).

Since oleate has been proposed to protect skeletal muscle cells from palmitate-induced apoptosis by promoting palmitate β-oxidation [25], we wondered whether oleate could counteract SFA-mediated NLRP3 inflammasome activation by the same way. Oleate co-treatment prevented stearate-induced IL-1β secretion but etomoxir had no effect on oleate-mediated inhibition (Fig. 3B). Altogether, these results demonstrate that β-oxidation does not play any role neither in the SFA-dependent NLRP3 inflammasome activation nor in its inhibition by oleate. Accordingly, we turned to the lipid synthesis, the second metabolic pathway involving fatty acyl-CoA.

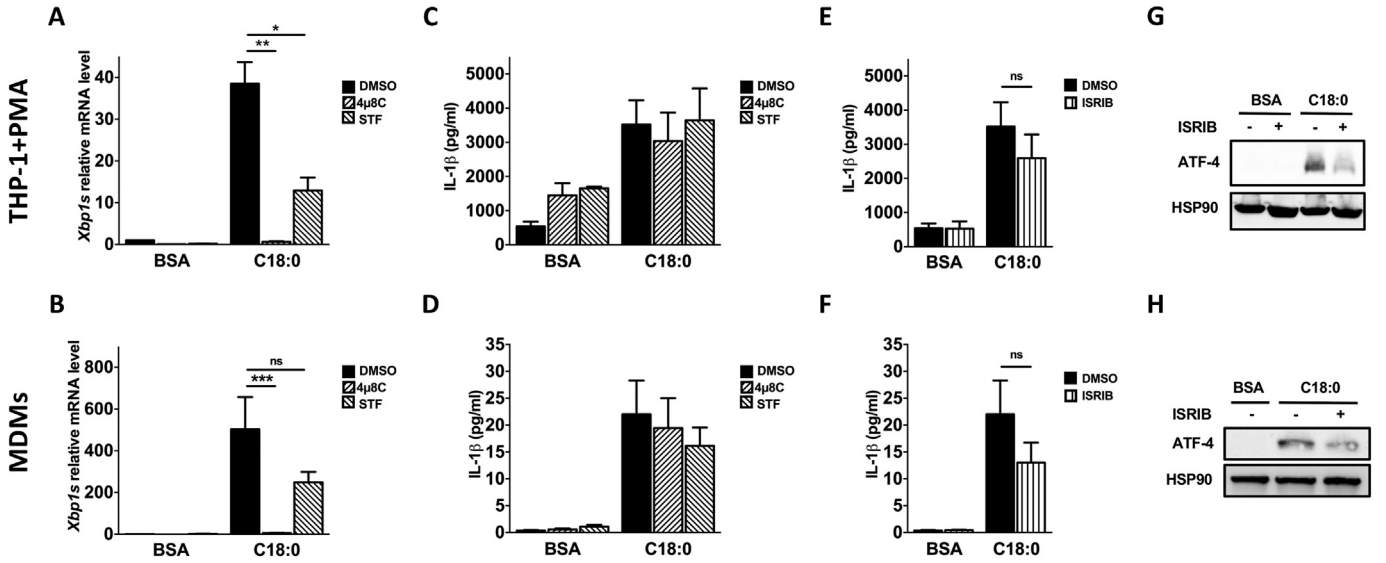


Fig. 2. IRE1α endoribonuclease activity is not required for C18:0-mediated NLRP3 inflammasome activation in human macrophages. Effects of IRE1α inhibitors (4μ8C and STF-083010) on spliced *Xbp1* mRNA expression (A, B) or IL-1β secretion (C, D) after C18:0 treatment. Effects of phosphorylated eIF2α inhibitor (ISRIB) on IL-1β secretion (E, F) and ATF4 expression (G, H) in response to C18:0. PMA-differentiated THP-1 cells or MDMs were pre-treated for 1 h with vehicle (DMSO) or with 4μ8C (50 μM), STF-083010 (STF, 100 μM) or ISRIB (10 nM) before addition of BSA (vehicle) or C18:0 (200 μM) for 8 h (THP-1 + PMA) or 16 h (MDMs). IL-1β was measured in supernatants by ELISA and relative spliced *Xbp1* mRNA expression was assessed by qRT-PCR. HSP90 and ATF-4 were detected by immunoblotting in PMA-differentiated THP-1 cells and MDMs extracts. Results are presented as means ± SEM of three (THP-1 + PMA) and four (MDMs) independent experiments. *P < 0.05; **P < 0.01; ***P < 0.001; ns, non-significant by two-way ANOVA followed by Bonferroni's post-hoc test.

3.3. Stearate is mainly incorporated in polar lipids but is redirected towards triacylglycerol in the presence of oleate

We followed the stearate flux by using radiolabeled stearate. The uptake of ^{14}C-labeled stearate by PMA-differentiated THP-1 cells linearly increased with time at least until 12 h and was only slightly affected by the presence of oleate, suggesting that the UFAs inhibiting effect on SFA-mediated NLRP3 inflammasome activation cannot be explained by a competition between SFAs and UFAs for cell internalization (Fig. 4A).

To assess the stearate flux into lipids, we treated PMA-differentiated THP-1 cells with stearate (200 μM) plus trace amounts of ^{14}C-labeled stearate for 8 h. Total lipids were extracted and labeled diacylglycerol (DAG), triacylglycerol (TAG), cholesterol esters and polar lipids were analyzed by TLC. When we focused on the ^{14}C-labeled stearate distribution among the lipid classes, we could see a major stearate incorporation in polar lipids (62% of the total lipid radioactivity) and to a lesser extent in TAG (27%) and DAG (11%) (Fig. 4B). Interestingly, when ^{14}C-labeled stearate was combined with oleate, ^{14}C-labeled polar lipids dramatically decreased (down to 25%), ^{14}C-labeled DAG disappeared whereas ^{14}C-labeled TAG significantly increased (up to 72%) (Fig. 4B).

The synthesis of TAG was also assessed by staining the lipid droplets (LD). A few small LD were observed after stearate treatment while oleate alone or combined with stearate triggered the formation of many bigger LDs confirming its efficiency to induce the synthesis of neutral lipids (Fig. 4C).

Altogether, these results suggest that stearate flux in PMA-differentiated THP-1 cells is mainly channeled towards polar lipids, while it is redirected towards TAG synthesis in the presence of oleate.

3.4. Stearate induces a strong phospholipid saturation correlated to a loss of membrane fluidity, both events reversed by oleate co-treatment

The different classes of phospholipids such as the phosphatidylcholine (PC), phosphatidylethanolamine (PE), phosphatidylserine (PS) and phosphatidylinositol (PI) were analyzed by mass spectrometry-based lipidomics. PC is far and away the most abundant phospholipids in all mammalian cell membranes. When we classified the individual PC species into saturated (no double bond), mono-unsaturated (double bond = 1) and poly-unsaturated (double bonds > 1) species, we observed a dramatic saturation of PC after stearate treatment (Fig. 5A). In control cells (BSA), most PC species were either mono-unsaturated (49.45%) or poly-unsaturated (40.01%) and only 10% carried no double bonds. The stearate treatment reversed the situation, making almost the half of the PC species saturated (46.35%), leaving only 33.41% and 20.24% of mono- and poly-unsaturated PC species, respectively (Fig. 5A). However, the oleate treatment only induced a slight decrease of saturated PC species (4.08%) compared to BSA control with a significant increase of poly-unsaturated ones (55.56%) (Fig. 5A). Interestingly, the combination of oleate with stearate prevented the strong stearate-mediated PC saturation that even tended towards a decrease (3.72%). The same trend was observed on the saturation profile of the three other classes, PE, PI and PS, whatever much less marked (data not shown).

The heatmap allows highlighting the ratios of the abundance of each phospholipid species (PC, PE, PS and PI) in FFA-treated cells over BSA control cells (Fig. 5B). As expected, the majority of the saturated species increased after stearate treatment, especially those with a total number of fatty acid carbons of 34 and 36 and this effect was reversed by oleate co-treatment. Some mono-unsaturated species such as those with 36, 38 and 40 carbons were also up-regulated by stearate and the combination stearate plus oleate but not with oleate alone. Overall, the poly-unsaturated species were down-regulated in response to stearate, mainly the first ones of each saturation class (32:2, 34:2, 32:3, 34:3, 34:4, 36:4, 36:5, 38:6…). This effect was also present but less marked with oleate alone and the combination stearate plus oleate.

Given the large increase in PC saturation after stearate treatment, we investigated its effects on the physical state of membranes by using the Laurdan fluorescence [26,27]. This probe tends to distribute evenly in lipid bilayers but its emission spectrum is influenced by the polarity of its environment; in apolar environments such as phospholipid bilayers in liquid ordered (Lo) or solid (So) phase enriched in saturated lipid species and cholesterol, its emission maximum is at 440 nm,

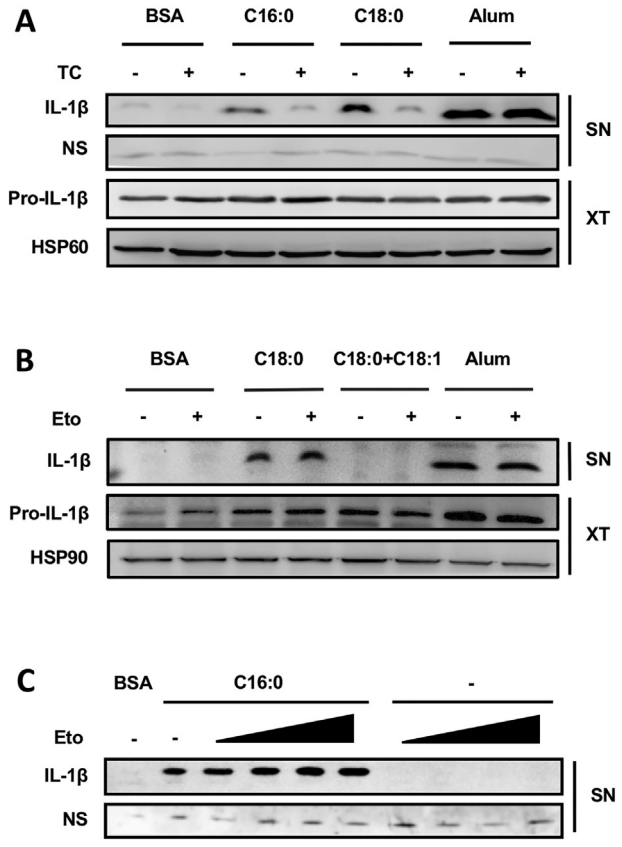


Fig. 3. SFAs activation into acyl-CoA is required for NLRP3 inflammasome activation but the β-oxidation is dispensable for both the SFA- and UFA-mediated effects. (A) SFAs activation into acyl-CoA is required for NLRP3 activation. (B, C) The SFAs flux in mitochondria is dispensable for both SFA-induced NLRP3 activation and UFA-mediated NLRP3 inhibition. PMA-differentiated THP-1 cells were pre-treated or not for 1 h with Triacsin C (TC, 5 μM) (A) or etomoxir (Eto, 25 μM) (B) before stimulation for 8 h with BSA, C16:0 (200 μM), C18:0 (200 μM) alone or in combination with C18:1 (200 μM + 200 μM) and Alum (400 μg/ml) or with increasing Eto concentrations (1, 10, 50 and 100 μM) (C) before stimulation with BSA or C16:0 (200 μM) for 8 h. IL-1β release in supernatant (SN) and the Pro-IL-1β, HSP60 or HSP90 levels in cytosol (XT) were determined by immunoblotting. A representative blot from minimal three independent experiments is shown. NS, non-specific band.

whereas in relatively polar environments such as membranes in liquid disordered state (Ld) comprising mainly unsaturated lipids, its emission maximum is at 490 nm. Generalized Polarization (GP) images can be constructed from the fluorescence intensity images obtained with blue and green band-pass filters on the microscope, allowing assessment of the phase state of the lipid domains. The GP images show that the PMA-differentiated THP-1 cells are relatively round with quite fluid membranes and some yellow intracytoplasmic vesicles (Fig. 6, BSA). The treatment with stearate (8 h) strongly affects the cell morphology, making their plasma membranes much less fluid. The number of vesicles is increased but they appear smaller (Fig. 6). However, oleate alone or in combination with stearate does not seem to disturb neither the cell morphology nor the lipid bilayers phase but induces an increase of both the number and the size of the yellow vesicles (Fig. 6). Such Laurdan-stained cytosolic vesicles were previously observed in other kinds of cells and were recently shown to be LD that are very apolar organelles [27]. Since we observed the accumulation of LD in PMA-differentiated THP-1 cells after treatment with oleate and the combination stearate plus oleate (Fig. 4C), we can consider these Laurdan-stained cytosolic vesicles like LD.

Altogether, the combined lipidomic and Laurdan fluorescence analyses demonstrated a chemical and physical membrane remodeling in stearate–treated macrophages-like cells, which can be prevented by the co-treatment with the corresponding mono-unsaturated fatty acid oleate.

3.5. *De novo* PC synthesis is required for SFA-mediated NLRP3 inflammasome activation

To prove that the mechanism underlying SFA-mediated NLRP3 activation requires the enrichment of saturated PC, we prevented *de novo* PC synthesis by knocking down the CTP:phosphocholine cytidylyltransferase alpha (CCTα) in PMA-differentiated THP-1 cells through their transfection with 2 different siRNAs. CCTα catalyses the rate-limiting step of the *de novo* PC synthesis (Fig. 7A) [28]. CCTα depletion was efficient with both siRNAs (Fig. 7B) and led to a significant downmodulation of the *de novo* PC synthesis, as demonstrated by the strong decrease of propargylcholine incorporation in macrophages (Fig. 7C). Interestingly, the disruption of the PC synthesis strongly affected the SFA-mediated NLRP3 activation as demonstrated by the significant decrease of IL-1β secretion, mainly in the case of stearate (Fig. 7D). While a slight decrease of pro-IL-1β levels was observed in siRNA CCTα1 (#1, #2)-transfected cells compared to siRNA CTR-transfected cells, these modulations can in no way explain the drop observed in the SFA-induced IL-1β secretion. Accordingly, this new rescue experiment demonstrates that PC synthesis has to be functional to allow stearate or palmitate incorporation leading to both saturated PC enrichment and loss of membrane fluidity. In the absence of exogenous stearate or palmitate (control BSA), *de novo* PC synthesis is effective in macrophages (Fig. 7C) but incorporates endogenous fatty acids coming from *de novo* synthesis *via* fatty acid synthase-dependent pathway or released from TAG hydrolysis, which ensures a low level of saturated PC (Fig. 5A). When SFA is added in the culture medium, this exogenous SFA in excess is preferentially incorporated into PC at the expense of endogenous fatty acid leading to PC saturation.

3.6. A K^+ efflux is essential and correlated to SFAs-mediated IL-1β release but reversed by UFA co-treatment

A K^+ efflux seems to be a common step to all NLRP3 inflammasome activation settings [15–17]. As expected, increasing extracellular K^+ concentrations from 5 to 55 mM had a dose-dependent inhibitory effect on NLRP3 activation by Alum in PMA-differentiated THP-1 cells (Fig. 8A). The same kind of effect, even more pronounced, was observed in the case of SFAs, demonstrating that a drop of cytosolic K^+ concentrations is also a requirement for SFAs-mediated NLRP3 activation both in PMA-differentiated THP-1 cells and MDMs (Fig. 8B). To establish a reliable correlation between intracellular K^+ concentrations and NLRP3 activation, we measured IL-1β release and K^+ efflux in parallel, in time-course experiments. As expected, both the extent and the kinetics of IL-1β release matched with the K^+ efflux in response to Alum, nigericin and ouabain (Na, K-ATPase inhibitor, [29,30]) (Fig. 8C). In comparison to these NLRP3 triggers, stearate induced a lower and slower drop of intracellular K^+ concentrations. Indeed, after 8 h, these K^+ concentrations reached 85% of K^+ control levels. Again, the K^+ efflux fitted with IL-1β production (Fig. 8D). Interestingly, oleate alone did not lead to a loss of intracellular K^+ and moreover, it prevented the stearate-mediated K^+ efflux, which correlated with its lack of effect or its inhibiting effect on IL-1β production, respectively. Oleate alone or in combination with stearate even tended to slightly increase intracellular K^+ concentrations (Fig. 8D). Altogether, these results demonstrate that SFAs induce a K^+ efflux that is required and correlated with IL-1β secretion, both events inhibited by UFAs.

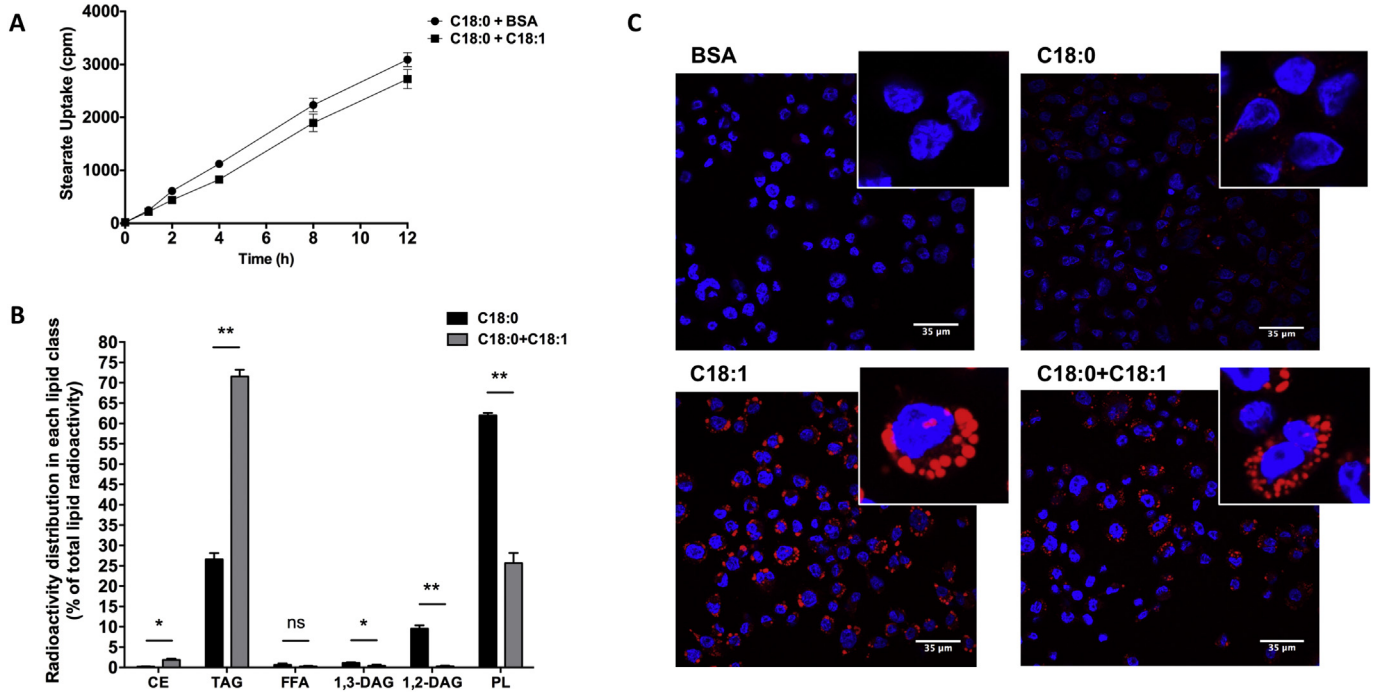


Fig. 4. Analysis of the C18:0 flux in the presence or not of C18:1. (A) C18:1 does not affect C18:0 uptake. PMA-differentiated THP-1 cells were treated with a mixture of 0,1 µCi/ml radiolabeled [1-14C] C18:0 and C18:0 (200 µM) in the presence or not of C18:1 (200 µM) during indicated times. Radioactivity in cell extracts was counted with liquid scintillation analyzer to evaluate the radiolabeled [1-14C] C18:0 uptake. Results are presented as means ± SEM of three independent experiments. (B) The C18:0 flux is mainly channeled towards polar lipids and redirected towards TAG in the presence of C18:1. PMA-differentiated THP-1 cells were treated with a mixture of 2 µCi/ml radiolabeled [1-14C] C18:0 and C18:0 (200 µM) in the presence or not of C18:1 (200 µM) during 8 h. Then total lipids were extracted and separated by TLC. Storage phosphor screens were exposed to the radioactive TLC for 4 h and scanned with Typhoon 9400™. Resulting digital image was quantified. Results are presented as means ± SEM of three independent experiments. *P < 0.05; **P < 0.01; ns, non-significant by *t*-test. (C) C18:1 induces LD formation. PMA-differentiated THP-1 cells were either treated with vehicle (BSA), with C18:0 (200 µM) or C18:1 (200 µM) alone or with the combination C18:0 + C18:1 (200 µM + 200 µM) during 8 h before being used for LD and nucleic acid staining with LipidTOX and DAPI, respectively. Representative images from minimal three independent experiments are shown. CE, cholesterol ester; TAG, triacylglycerol; FFA, free fatty acid; 1,3-DAG, 1,3-diacylglycerol; 1,2-DAG, 1,2-diacylglycerol; PL, polar lipids.

3.7. A disruption of the plasma membrane Na, K-ATPase is induced by SFAs and prevented by UFAs co-treatment

The Na, K-ATPase maintains the Na, K gradient across the plasma membrane by shuttling 2 K^+ in the cell and releasing 3 Na^+ outside. Its activity is known to be modulated both by biophysical properties of the plasma membrane and specific interactions with phospholipids [31]. The down-regulation of the Na, K-ATPase has already been shown able to induce NLRP3 activation [29,30]. Ouabain, a specific inhibitor of the Na, K-ATPase, leads to a strong K^+ efflux associated to a significant NLRP3 inflammasome activation (Fig. 8C). For all these reasons, we tested the effect of the different SFA/UFA treatments on Na, K-ATPase activity that we estimated by the ouabain sensitive-$^{86}Rb^+$ uptake. The activity of the Na, K-ATPase was down-regulated to 92% and 88% with palmitate (200 µM, 8 h) and stearate (200 µM, 8 h), respectively, while the Na, K-ATPase α1 catalytic subunit levels in the membrane remained unchanged after the various treatments (Fig. 9A). Furthermore, the ouabain sensitive-$^{86}Rb^+$ uptake was not affected by oleate alone and tended to slightly increase with the combination stearate plus oleate (103%) (Fig. 9A). Interestingly, the activity of the Na, K-ATPase seems to be correlated to intracellular K^+ concentrations shown in Fig. 8D. Both SFAs also disrupted the Na, K-ATPase pump in MDMs; palmitate (400 µM, 8 h) and stearate (400 µM, 8 h) reduced the activity of the Na, K-ATPase to 77% and 76.5%, respectively, without modifying the protein levels in the plasma membrane (Fig. 9B).

4. Discussion

Nowadays, a high percentage of mortality in Western countries is due to chronic diseases like type 2 diabetes, obesity and cardiovascular diseases that are influenced by eating habits. NLRP3 plays a key role in the development of these Western diet (WD)-associated diseases by sensing sterile danger signals and triggering systemic inflammation. Very recently, a notable study demonstrated that WD, in addition to induce systemic inflammation, instigates a long-lasting trained immunity through NLRP3-dependent myeloid cells reprogramming [32]. In light of these recent data, there is a great interest in understanding how WD activates the NLRP3 inflammasome. SFAs have been proposed as NLRP3 metabolic triggers [10–12]. We also previously demonstrated both the activating effect of SFAs and the protective effect of UFAs on NLRP3 inflammasome activation in human macrophages [21]. Here, we show the important role of the SFAs flux towards phospholipids leading to a loss of membrane fluidity and a K^+ efflux correlated to the Na, K-ATPase disruption. Interestingly, all these events are reversed by UFAs that redirect the SFA flux towards TAG.

Prior studies have involved mROS accumulation due to impairment of AMPK-regulated autophagy in the palmitate-mediated NLRP3 activation in LPS-primed BMDMs [12]. Others showed mROS production after palmitate treatment of LPS-primed murine peritoneal macrophages but the mitochondrial antioxidant MitoTEMPO failed to inhibit the palmitate-mediated IL-1β release [33]. We did not observe ROS production neither in PMA-differentiated THP-1 cells nor in MDMs after both palmitate and stearate treatments.

More recently, the IRE1α-dependent UPR branch was proposed to mediate the SFA-induced NLRP3 inflammasome activation in LPS-primed BMDCs [20]. Indeed, Robblee et al. demonstrated that both inhibitors of IRE1α endoribonuclease activity (4μ8C and STF-083010) decreased the extent to which SFA treatment induced both *Xbp1*

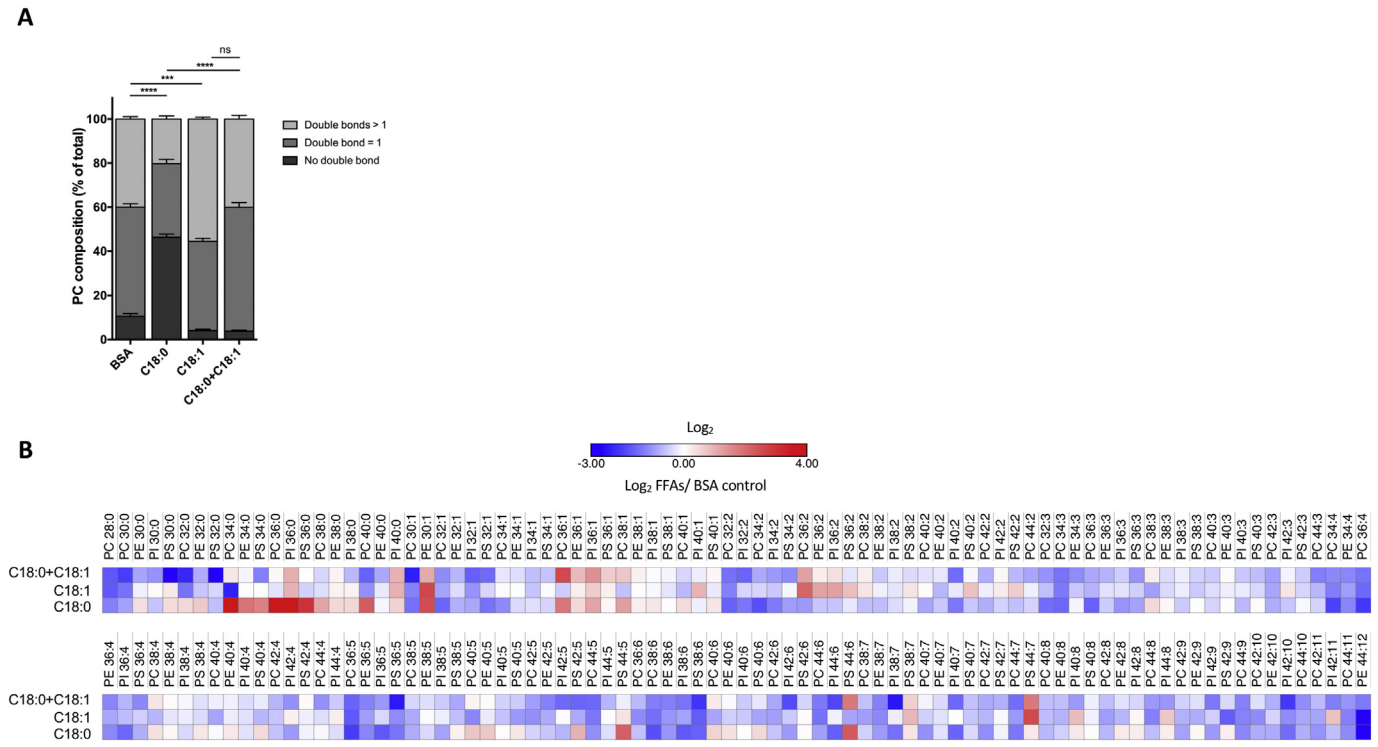


Fig. 5. C18:0 induces a dramatic increase in saturated PC that is prevented by C18:1 co-treatment. PMA-differentiated THP-1 cells were treated with BSA (vehicle), C18:0 (200 µM) or C18:1 (200 µM) alone or in combination C18:0 + C18:1 (200 µM + 200 µM) for 8 h. Lipid extracts were used for lipidomic analysis. (A) The percentages of saturated (double bond = 0), mono-unsaturated (double bond = 1) and poly-unsaturated (double bond > 1) PC were calculated for each treatment. Results are presented as means ± SEM of three independent experiments. Percentages of saturated PC were compared between the different treatments by two-way ANOVA followed by Tukey's post-hoc test (***P < 0.001; ****P < 0.0001; ns, non-significant). (B) Heatmap of $\log_2$ ratios of the abundance of phospholipids species in FFAs-treated PMA-differentiated THP-1 cells over vehicle (BSA)-treated cells. $\log_2$ fold change was arbitrarily set at −3.00/4.00 for coloring. Lipid species are indicated by their total number of fatty acid carbons, followed by the total number of unsaturations.

splicing and IL-1β secretion. IRE1α is known to be activated by the recognition of unfolded proteins in ER lumen but compelling evidences suggest that IRE1 is also able to sense ER lipid bilayer stress [10,34]. Authors demonstrated through TLC performed on lipid extracts of radiolabeled palmitate-treated BMDCs that palmitate is mainly incorporated into PC. Limiting PC synthesis by chemical inhibitors reduced the ability of both palmitate and stearate to induce *Xbp1* splicing and IL-1β secretion, suggesting that incorporation of SFAs into ER membrane PC contributes to the activation of both IRE1α and NLRP3 pathways. However, the mechanism by which the SFA-induced IRE1α-XBP1 pathway could lead to NLRP3 inflammasome activation still remains unknown. We also observed a strong and rapid activation of the PERK-EIF2α-ATF4 and IRE1α-XBP1 pathways in our both stearate-treated human macrophage models. However, both STF-083010 and 4μ8C had no effect on stearate-mediated NLRP3 activation neither in PMA-differentiated THP-1 cells nor in MDMs while they induced a significant decrease of *Xbp-1* mRNA splicing. These opposing data concerning involvement of both ROS and IRE1α could be explained by the use of various macrophage models, either resting or LPS-primed and by the selection of different treatment conditions such as the kind of SFA (palmitate or stearate), the SFA concentration and treatment time. We definitively think that LPS pre-treatment, by rapidly inducing the expression of many genes such as those involved in some metabolic pathways [35], could really influence the FFA signaling inside macrophages.

By using inhibitors of ACSLs (Triacsin C) and CPT1 (etomoxir), we demonstrated that both palmitate and stearate have to be activated into acyl-CoA but do not need to enter the mitochondria to induce NLRP3 inflammasome activation. Accordingly, fatty acid oxidation seems to be dispensable for NLRP3 inflammasome activation in SFA-treated human macrophages unlike other NLRP3 activation settings [36]. Moreover, preventing palmitate to enter the mitochondria had even an upregulating effect on NLRP3-mediated IL-1β release. Etomoxir probably induced a redirection of the palmitate flux towards another metabolic pathway like lipid synthesis favoring NLRP3 inflammasome activation. This synergistic effect of etomoxir was only obtained with palmitate and not with stearate. This observation allows us to suggest that, in human macrophages, palmitate is a less efficient NLRP3 trigger than stearate because its flux is more important towards β-oxidation at the expense of the lipid synthesis. Interestingly, this exacerbating effect of etomoxir has been already observed on palmitate-induced inflammatory and ER stress responses in human macrophages [37].

When we followed the incorporation of radiolabeled stearate in lipids, we also observed a major incorporation into polar lipids. We then determined the phospholipid composition of macrophages' membrane by lipidomic analysis after the different treatments with SFA and/or UFA. We observed a rapid and dramatic increase of saturated phospholipids especially in the case of the PC, which consisted of almost 50% saturated species after 8 h treatment with stearate compared to 10% in BSA condition. Interestingly, inhibiting the *de novo* PC synthesis by knocking down the key enzyme CCTα was able to prevent SFA-mediated NLRP3 inflammasome activation.

The heatmap revealed an increase of saturated species but also an up-regulation of some mono-unsaturated ones with an overall reduction of the poly-unsaturated species, a pattern that corresponds to the *de novo* lipogenesis profile [38]. Indeed, an ongoing analysis of the whole transcriptome of stearate-treated MDMs allowed us to identify an up-regulation of some genes involved in *de novo* lipogenesis and glycerolipid synthesis already after 8 h treatment. The dramatic increase observed in the saturation of phospholipids could be explained not only by an exogenous stearate uptake but also by increased *de novo* lipogenesis and glycerolipid synthesis. Such hypothesis needs further investigation.

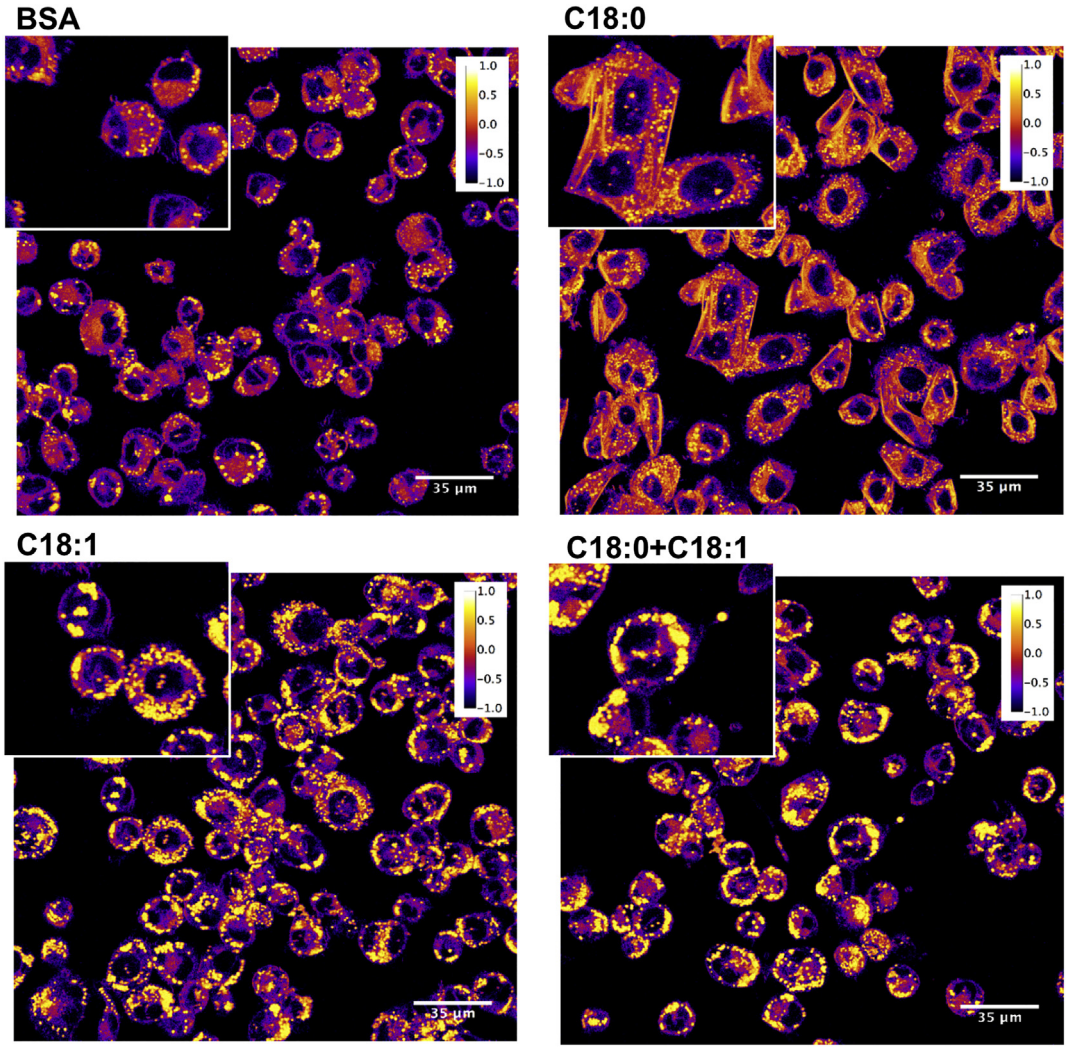


Fig. 6. A strong decrease in membrane fluidity is induced by C18:0 but reversed by C18:1 co-treatment. PMA-differentiated THP-1 cells were either treated with vehicle (BSA), with C18:0 (200 µM) and with C18:1 (200 µM) alone or in combination C18:0 + C18:1 (200 µM + 200 µM) during 8 h. After treatment, living cells were labeled with Laurdan (2,5 µM) for 1 h and two-photon excitation microscopy was performed at room temperature. GP images of living cells were generated using the images acquired simultaneously in the two Laurdan emission spectra applying the GP formula and using ImageJ. Representative images from minimal three independent experiments are shown. The colors indicate different GP values according to the reported scale going from 1 (gel phase) to −1 (fluid phase).

It is well-known that unsaturated lipids with a kinked shape create a liquid-disordered phase while saturated fatty acyl chains, straight and closely packed, lead to a thicker membrane characterized by a liquid-ordered phase [39,40]. As expected, we observed, through the Laurdan fluorescence, a radical and rapid decrease of the membrane fluidity of human macrophages. It is usually accepted that both the membrane biophysical properties and the lipid composition can modulate the activity of integral proteins through various mechanisms [39,41,42].

The plasma membrane Na, K-ATPase is an integral protein whose activity is affected by membrane remodeling [31]. Its α catalytic subunit comprises 10 transmembrane helices required for ion binding and three cytosolic domains mediating ATP binding, ATP hydrolyzing activity or carrying phosphorylation sites. The Na, K-ATPase is a member of the P-type ATPase family characterized by ATP-dependent cyclic transition between two different conformational states, E1 and E2, which binds three Na^+ and two K^+, respectively. The Na, K-ATPase insertion into liposomes of defined lipid composition allowed showing the modulation of its pump activity by the physical properties of the lipid bilayer [31]. Later, through crystallization and biochemical studies, three pockets were resolved in the transmembrane domain that specifically bind anionic lipids, polyunsaturated neutral phospholipids and saturated PC conferring, respectively, stabilizing, stimulating and inhibiting effects on the Na, K-ATPase activity [31,43,44]. Interestingly, the Na, K-ATPase activity is decreased in erythrocytes showing a higher saturation level of membrane phospholipids in hypertension cases [45,46]. For all these reasons and because we showed a dramatic increase in PC saturation closely correlated to both a K^+ efflux and NLRP3 inflammasome activation in SFA-treated human macrophages, we turned to the Na, K-ATPase. As expected, we observed a reduction of the K^+ uptake by the Na, K-ATPase in SFA-treated human macrophages. Therefore, we propose the following model: in SFA-treated human macrophages, strongly increased saturated PC, by reducing the membrane fluidity and/or by modulating the lipid bilayer thickness or even through direct inhibiting interactions disrupt the plasma membrane Na, K-ATPase activity, which leads to a K^+ efflux followed by NLRP3 inflammasome activation. The link between all these events is reinforced by the rescue effect of UFAs on each step. Since the lipidomic analysis was performed on total lipid extracts, we cannot exclude the possibility that ER or mitochondria membranes are also damaged by the SFA treatment leading to the disruption of sarco/endoplasmic reticulum Ca^{2+} ATPase (SERCA)-mediated Ca^{2+} homeostasis or mitochondrial dysfunction, both events previously related to NLRP3 activation [8].

We also investigated the mechanism by which UFAs prevent SFAs-mediated NLRP3 activation. Oleate does not compete with stearate to

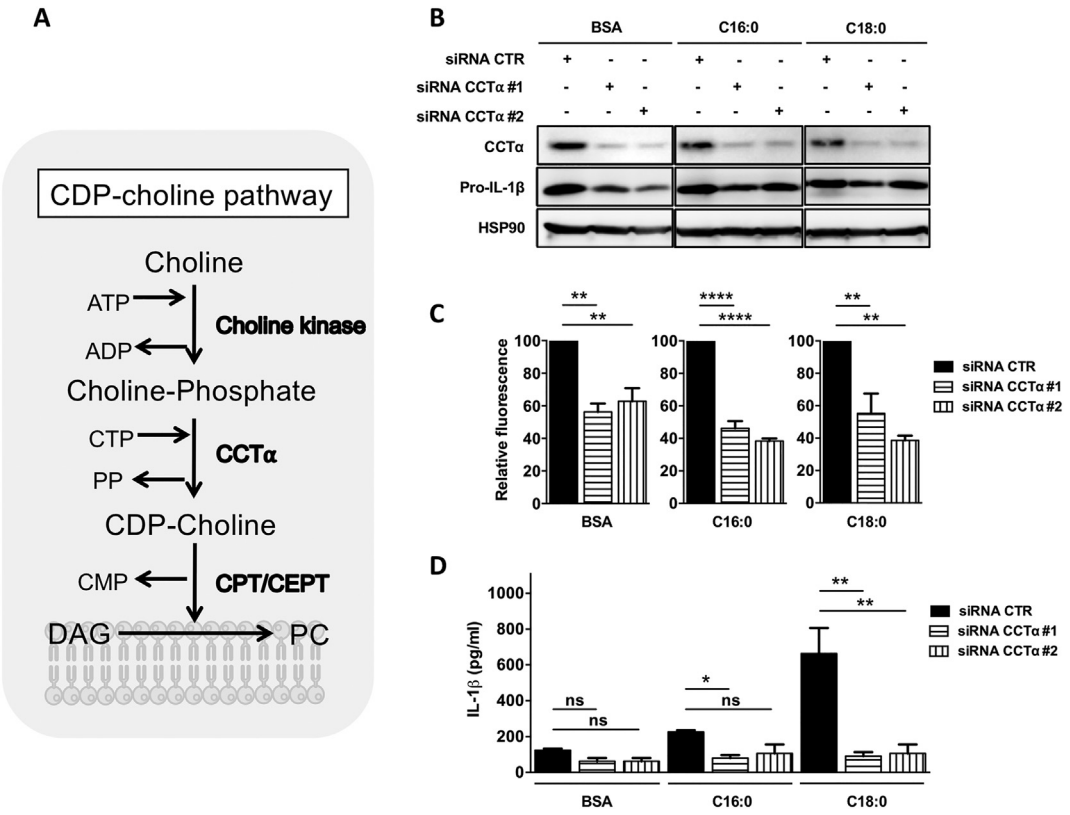


Fig. 7. CCTα-dependent *de novo* PC synthesis is required for SFA-mediated NLRP3 activation. (A) CDP-choline pathway for PC synthesis. CPT, CDP-choline phosphotransferase; CEPT, CDP-choline/ethanolamine phosphotransferase. (B, C, D) PMA-differentiated THP-1 cells were treated with BSA or SFAs (200 μM) for 8 h after CCTα silencing by siRNAs. (B) CCTα, Pro-IL-1β and HSP90 levels in total lysates were determined by immunoblotting. A representative blot from minimal three independent experiments is shown. (C) Neo-synthetized PCs (% of siRNA CTR condition) were monitored in fixed cells using click chemistry reaction between Propargylcholine and Alexa Fluor 488 azide. Results are presented as means ± SEM of three independent experiments. **P < 0.01; ****P < 0.0001 by one-way ANOVA followed by Dunnett's post-hoc test. (D) IL-1β was measured in supernatants by ELISA. Results are presented as means ± SEM of three independent experiments. *P < 0.05; **P < 0.01; ns, non-significant by one-way ANOVA followed by Dunnett's post-hoc test.

enter the macrophages, does not mediate its inhibiting effect by increasing the mitochondrial stearate flux but redirects the stearate flux from polar lipids to TAG stored in LD, thereby preventing the saturation of PC, the Na, K-ATPase disruption, the K^+ efflux and NLRP3 inflammasome activation.

Results from this manuscript combined with data from the literature allow us to recapitulate the FFA flux occurring in human macrophages after different FFA treatments. In the absence of exogenous stearate or palmitate (control BSA), *de novo* PC synthesis is effective in macrophages (Fig. 7C) but incorporates endogenous fatty acids coming from *de novo* synthesis *via* fatty acid synthase-dependent pathway or released from TAG hydrolysis, which ensures a low level of saturated PC (Fig. 5A). When stearate is added in the culture medium, this exogenous SFA in excess is preferentially incorporated into PC at the expense of endogenous FA leading to PC saturation. A much smaller amount of exogenous stearate is also incorporated in TAG (Fig. 4B). The addition of exogenous oleate, while slightly modulating the abundance of some phospholipid species (Fig. 5B), strongly stimulates the TAG synthesis as demonstrated by the appearance of many large lipid droplets (Fig. 4C). The esterification of a fatty acyl moiety to DAG to form TAG is catalysed by two diacylglycerol O-acyltransferases, DGAT1 and DGAT2. Both proteins are ER transmembrane proteins. Their different membrane topologies give them different abilities to interact with other proteins and organelles and access to different pools of fatty acids; DGAT1 is proposed to have dual topology contributing to TAG synthesis on both sides of the ER membrane and esterifying only exogenous fatty acids. DGAT2 translocates to LD, associates with other proteins, and synthesizes TAG from both endogenous and exogenous fatty acids [47]. A model of DGAT1 activation was proposed [48]; the enzyme initially exists in the inactive state through the binding of high CoA levels to the allosteric site. CoA can be displaced through increased availability of acyl-CoA, allowing both conformational changes and activation of DGAT1. Accordingly, when stearate is added with oleate, exogenous fatty acids concentrations increase, further boosting DGAT1 activity and directing both FFAs flux towards TAG (Fig. 4B), which prevents PC saturation (Fig. 5A) and all the stearate-triggered downstream steps leading to NLRP3 activation (Figs. 8–9).

In attempt to reverse the “protective” effect of oleate, we tried to prevent this oleate-mediated switch in stearate flux by inhibiting DGAT1 or DGAT2. Interestingly, in the presence of DGAT1 inhibitor, the incorporation of radiolabeled stearate when combined with oleate decreased in TAG while re-increasing in polar lipids (data not shown). DGAT2 inhibition had no effect on stearate flux (data not shown). However, the redirection of stearate towards polar lipids after DGAT1 inhibition did not allow to restore NLRP3 inflammasome activation probably because oleate was also channeled towards phospholipids, preventing the dramatic increase of saturated PC. Nevertheless, this experiment shows that DGAT1 mediates the oleate inhibiting effect on stearate-induced NLRP3 activation. Robblee et al. did not observe any impact of oleate co-treatment on palmitate flux into lipids maybe because they used five-fold more palmitate than oleate while we always treated macrophages with equimolar stearate and oleate concentrations.

WD is characterized by high levels of both saturated fat and carbohydrates. These latter supply the *de novo* lipogenesis in liver and adipocytes generating SFAs that are released throughout the body *via*

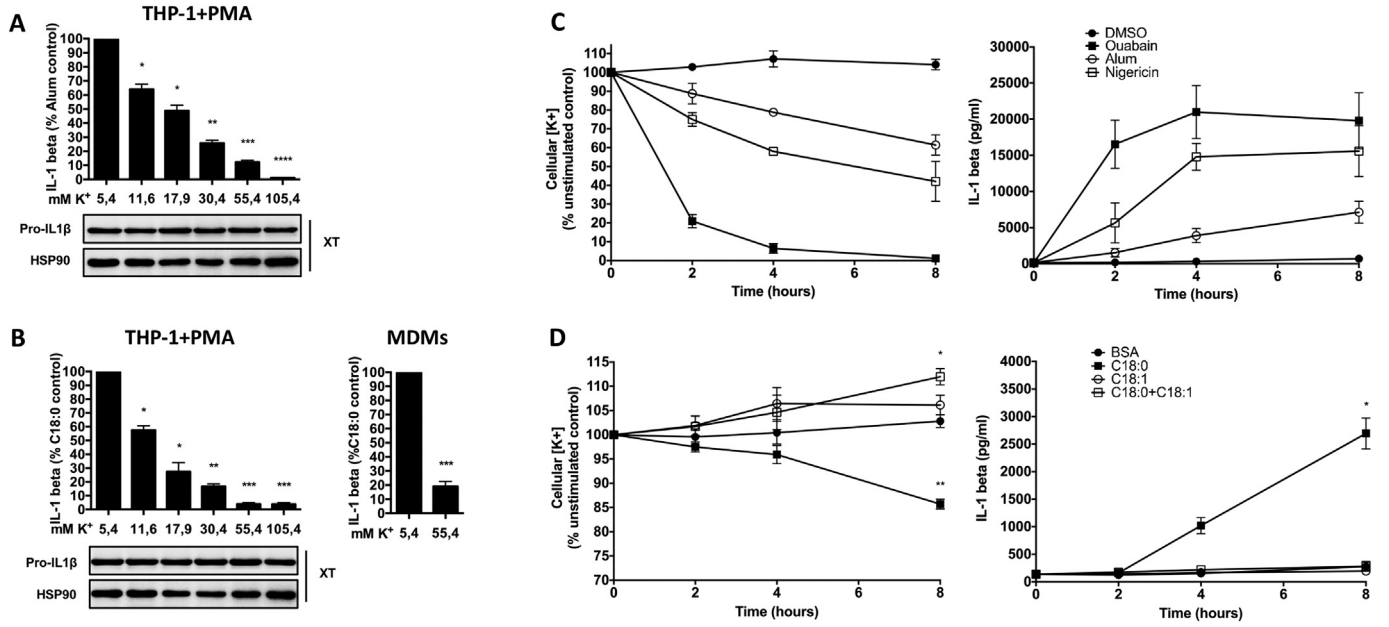


Fig. 8. C18:0 induces a K^+ efflux that is essential and closely correlated with IL-1β release. (A, B) The K^+ efflux is an essential step. (A) PMA-differentiated THP-1 cells were treated with Alum (400 μg/ml) in presence of increasing extracellular [K^+]. (B) Both PMA-differentiated THP-1 cells and MDMs were stimulated with C18:0 (200 μM) in presence of increasing extracellular [K^+] during 8 or 16 h, respectively. Supernatants (SNs) were harvested for IL-1β measurements by ELISA. The levels of Pro-IL-1β and HSP90 in cytosol (XT) were determined by immunoblotting. Results are presented as means ± SEM of three (PMA-differentiated THP-1 cells) or four (MDMs) independent experiments. *P < 0.05; **P < 0.01; ***P < 0.001; ****P < 0.0001 by one-way ANOVA followed by Dunnett's post-hoc test (PMA-differentiated THP-1 cells). ***P < 0.001 by *t*-test (MDMs). (C, D) The K^+ efflux is tightly correlated to IL-1β secretion. (C) PMA-differentiated THP-1 cells were either treated with vehicle (DMSO), Alum (400 μg/ml), nigericin (10 μM) or ouabain (1 μM) or (D) with BSA, C18:0 (200 μM) or C18:1 (200 μM) alone or in combination C18:0 + C18:1 (200 μM + 200 μM) during indicated times. SNs were harvested for IL-1β measurements by ELISA and cell lysates in 10% nitric acid were analyzed by atomic emission spectroscopy to determine intracellular [K^+]. Results are presented as means ± SEM of three independent experiments. *P < 0.05; **P < 0.01 by one-way ANOVA followed by Tukey's post-hoc test.

lipoproteins or as free fatty acids [49]. The composition of membrane phospholipids was reported to be influenced by the fatty acid composition of the diet [50–52]. These observations combined with compelling evidence of the NLRP3 central role in WD-induced systemic inflammation highlight the relevance of this NLRP3 activation model based on membrane saturation.

Obesity is also characterized by an accumulation of FFAs in the plasma and insulin-target tissues [53]. Membrane modifications in both fluidity and lipid composition have been observed in several types of cells in patients with T2D [54–57]. SFAs levels in red blood cells membranes have been also correlated with the susceptibility to develop T2D [58,59]. In addition to the Na, K-ATPase, several integral membrane proteins involved in inflammatory and metabolic pathways such as TLR4, SERCA, IRE1α, …are also modulated by the disruption of the membrane homeostasis and relevant in the context of obesity [39]. The "membrane-centric view of T2D" is reinforced by this study demonstrating that NLRP3, a central effector in the development of obesity-related inflammation and insulin resistance, also senses membrane damage. This work leads to novel therapeutic avenues such as those targeting the glycerolipid pathway.

Transparency document

The Transparency document associated with this article can be found, in online version.

Acknowledgments

This work was supported by the Belgian F.R.S.-FNRS, the Leon Fredericq funds for Biomedical Research from the University of Liège,

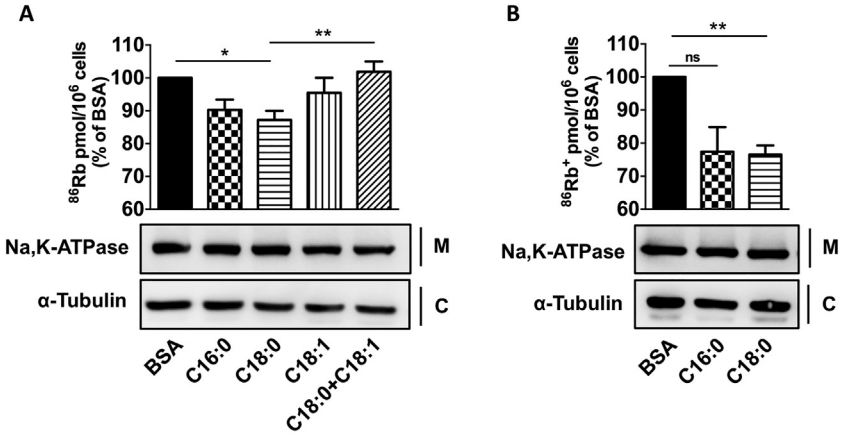


Fig. 9. The activity of the plasma membrane Na, K-ATPase is down-regulated by SFAs treatment. (A) PMA-differentiated THP-1 cells were either treated with vehicle (BSA), with C16:0 (200 μM), C18:0 (200 μM), C18:1 (200 μM) or with the combination C18:0 + C18:1 (200 μM + 200 μM) during 8 h. (B) MDMs were either treated with vehicle (BSA), C16:0 (400 μM) or C18:0 (400 μM) during 8 h. The Na, K-ATPase activity was estimated by ouabain-sensitive $^{86}Rb^+$ uptake. The levels of the Na, K-ATPase α1 subunit and α-Tubulin were determined by immunoblotting on membrane (M) and cytoplasmic (C) cell fractions, respectively. Results are presented as means ± SEM of five (PMA-differentiated THP-1 cells) or four (MDMs) independent experiments. *P < 0.05; **P < 0.01 by one-way ANOVA followed by Tukey's post-hoc test (PMA-differentiated THP-1 cells). **P < 0.01; ns, non-significant by one-way ANOVA followed by Dunnett's post-hoc test (MDMs).

Belgium and the Interuniversity Attraction Poles program (IAP7/342). S.L.-P., Y.H. and J.P. are Research Associate, Senior Research Associate and Honorary Research Director of the Belgian F.R.S.-FNRS, respectively. M.A.G. received a PhD fellowship from Walloon Region. The authors thank the Cell and Tissue Imaging Core (CIC, Impulse Financing KU Leuven, 2004) for the use of two-photon excitation microscope, and the GIGA Cell Imaging and Flow Cytometry Platforms. We are grateful to Jean-François Liégeois, Research Director of the Belgian F.R.S.-FNRS for the use of liquid scintillation analyzer and stearate uptake experiment setups. We also thank Michel Frédérich (University of Liège), for the help with TLC experiments.

Authors contribution

M.A.G. performed experiments. M.A.G. and S. L-P. conceived, designed the experiments, analyzed the data and wrote the manuscript. J.P., N.P. and L.L. contributed to the conception and design of the study. J.D. and J.V.S. contributed to the acquisition, analysis and interpretation of lipidomic and Laurdan microscopy data. N.E., Y.H., C.L., G.H., and O.J. contributed to helpful technical discussion or assistance. All authors revised and approved the manuscript. The authors declare that there is no conflict of interest associated with this manuscript.

References

[1] R.H. Eckel, S.M. Grundy, P.Z. Zimmet, The metabolic syndrome, Lancet Lond. Engl. 365 (2005) 1415–1428, https://doi.org/10.1016/S0140-6736(05)66378-7.
[2] A.H. Mokdad, E.S. Ford, B.A. Bowman, W.H. Dietz, F. Vinicor, V.S. Bales, J.S. Marks, Prevalence of obesity, diabetes, and obesity-related health risk factors, JAMA. 289 (2003) (2001) 76–79, https://doi.org/10.1001/jama.289.1.76.
[3] N. Esser, S. Legrand-Poels, J. Piette, A.J. Scheen, N. Paquot, Inflammation as a link between obesity, metabolic syndrome and type 2 diabetes, Diabetes Res. Clin. Pract. 105 (2014) 141–150, https://doi.org/10.1016/j.diabres.2014.04.006.
[4] J. Jager, T. Grémeaux, M. Cormont, Y. Le Marchand-Brustel, J.-F. Tanti, Interleukin-1beta-induced insulin resistance in adipocytes through down-regulation of insulin receptor substrate-1 expression, Endocrinology. 148 (2007) 241–251, https://doi.org/10.1210/en.2006-0692.
[5] K. Maedler, P. Sergeev, F. Ris, J. Oberholzer, H.I. Joller-Jemelka, G.A. Spinas, N. Kaiser, P.A. Halban, M.Y. Donath, Glucose-induced beta cell production of IL-1beta contributes to glucotoxicity in human pancreatic islets, J. Clin. Invest. 110 (2002) 851–860, https://doi.org/10.1172/JCI15318.
[6] K. Schroder, J. Tschopp, The inflammasomes, Cell. 140 (2010) 821–832, https://doi.org/10.1016/j.cell.2010.01.040.
[7] P. Broz, V.M. Dixit, Inflammasomes: mechanism of assembly, regulation and signalling, Nat. Rev. Immunol. 16 (2016) 407–420, https://doi.org/10.1038/nri.2016.58.
[8] T. Horng, Calcium signaling and mitochondrial destabilization in the triggering of the NLRP3 inflammasome, Trends Immunol. 35 (2014) 253–261, https://doi.org/10.1016/j.it.2014.02.007.
[9] M.Y. Donath, É. Dalmas, N.S. Sauter, M. Böni-Schnetzler, Inflammation in obesity and diabetes: islet dysfunction and therapeutic opportunity, Cell Metab. 17 (2013) 860–872, https://doi.org/10.1016/j.cmet.2013.05.001.
[10] S. Legrand-Poels, N. Esser, L. L'homme, A. Scheen, N. Paquot, J. Piette, Free fatty acids as modulators of the NLRP3 inflammasome in obesity/type 2 diabetes, Biochem. Pharmacol. 92 (2014) 131–141, https://doi.org/10.1016/j.bcp.2014.08.013.
[11] B. Vandanmagsar, Y.-H. Youm, A. Ravussin, J.E. Galgani, K. Stadler, R.L. Mynatt, E. Ravussin, J.M. Stephens, V.D. Dixit, The NALP3/NLRP3 inflammasome instigates obesity-induced autoinflammation and insulin resistance, Nat. Med. 17 (2011) 179–188, https://doi.org/10.1038/nm.2279.
[12] H. Wen, D. Gris, Y. Lei, S. Jha, L. Zhang, M.T. Huang, W.J. Brickey, J.P. Ting, Fatty acid-induced NLRP3-ASC inflammasome activation interferes with insulin signaling, Nat. Immunol. 12 (2011) 408–415, https://doi.org/10.1038/ni.2022.
[13] N. Esser, L. L'homme, A.D. Roover, L. Kohnen, A.J. Scheen, M. Moutschen, J. Piette, S. Legrand-Poels, N. Paquot, Obesity phenotype is related to NLRP3 inflammasome activity and immunological profile of visceral adipose tissue, Diabetologia. 56 (2013) 2487–2497, https://doi.org/10.1007/s00125-013-3023-9.
[14] H. Guo, J.B. Callaway, J.P.-Y. Ting, Inflammasomes: mechanism of action, role in disease, and therapeutics, Nat. Med. 21 (2015) 677–687, https://doi.org/10.1038/nm.3893.
[15] R. Muñoz-Planillo, P. Kuffa, G. Martínez-Colón, B.L. Smith, T.M. Rajendiran, G. Núñez, K+ efflux is the common trigger of NLRP3 inflammasome activation by bacterial toxins and particulate matter, Immunity. 38 (2013) 1142–1153, https://doi.org/10.1016/j.immuni.2013.05.016.
[16] L. Franchi, T. Eigenbrod, R. Muñoz-Planillo, U. Ozkurede, Y.-G. Kim, A. Chakrabarti, M. Gale, R.H. Silverman, M. Colonna, S. Akira, G. Núñez, Cytosolic double-stranded RNA activates the NLRP3 inflammasome via MAVS-induced membrane permeabilization and K+ efflux, J. Immunol. 193 (2014) 4214–4222, https://doi.org/10.4049/jimmunol.1400582.
[17] T. Próchnicki, M.S. Mangan, E. Latz, Recent insights into the molecular mechanisms of the NLRP3 inflammasome activation, F1000Research. 5 (2016). doi:10.12688/f1000research.8614.1.
[18] J. Chen, Z.J. Chen, PtdIns4P on dispersed trans-Golgi network mediates NLRP3 inflammasome activation, Nature. 564 (2018) 71–76, https://doi.org/10.1038/s41586-018-0761-3.
[19] Y. He, M.Y. Zeng, D. Yang, B. Motro, G. Núñez, Nek7 is an essential mediator of NLRP3 activation downstream of potassium efflux, Nature. 530 (2016) 354–357, https://doi.org/10.1038/nature16959.
[20] M.M. Robblee, C.C. Kim, J.P. Abate, M. Valdearcos, K.L.M. Sandlund, M.K. Shenoy, R. Volmer, T. Iwawaki, S.K. Koliwad, Saturated fatty acids engage an IRE1α-dependent pathway to activate the NLRP3 inflammasome in myeloid cells, Cell Rep. 14 (2016) 2611–2623, https://doi.org/10.1016/j.celrep.2016.02.053.
[21] L. L'homme, N. Esser, L. Riva, A. Scheen, N. Paquot, J. Piette, S. Legrand-Poels, Unsaturated fatty acids prevent activation of NLRP3 inflammasome in human monocytes/macrophages, J. Lipid Res. 54 (2013) 2998–3008, https://doi.org/10.1194/jlr.M037861.
[22] G. Liebisch, B. Lieser, J. Rathenberg, W. Drobnik, G. Schmitz, High-throughput quantification of phosphatidylcholine and sphingomyelin by electrospray ionization tandem mass spectrometry coupled with isotope correction algorithm, Biochim. Biophys. Acta BBA - Mol. Cell Biol. Lipids. 1686 (2004) 108–117, https://doi.org/10.1016/j.bbalip.2004.09.003.
[23] K.J. Livak, T.D. Schmittgen, Analysis of relative gene expression data using real-time quantitative PCR and the 2(−delta delta C(T)) method, Methods San Diego Calif, 25 (2001), pp. 402–408, https://doi.org/10.1006/meth.2001.1262.
[24] T.J. Grevengoed, E.L. Klett, R.A. Coleman, Acyl-CoA metabolism and partitioning, Annu. Rev. Nutr. 34 (2014) 1–30, https://doi.org/10.1146/annurev-nutr-071813-105541.
[25] C. Henique, A. Mansouri, G. Fumey, V. Lenoir, J. Girard, F. Bouillaud, C. Prip-Buus, I. Cohen, Increased mitochondrial fatty acid oxidation is sufficient to protect skeletal muscle cells from palmitate-induced apoptosis, J. Biol. Chem. 285 (2010) 36818–36827, https://doi.org/10.1074/jbc.M110.170431.
[26] A.G. Jay, J.A. Hamilton, Disorder amidst membrane order: standardizing laurdan generalized polarization and membrane fluidity terms, J. Fluoresc. 27 (2017) 243–249, https://doi.org/10.1007/s10895-016-1951-8.
[27] S. Mazeres, F. Fereidouni, E. Joly, Using spectral decomposition of the signals from laurdan-derived probes to evaluate the physical state of membranes in live cells, F1000Research. 6 (2017) 763. doi:10.12688/f1000research.11577.2.
[28] R.B. Cornell, N.D. Ridgway, CTP:phosphocholine cytidylyltransferase: function, regulation, and structure of an amphitropic enzyme required for membrane biogenesis, Prog. Lipid Res. 59 (2015) 147–171, https://doi.org/10.1016/j.plipres.2015.07.001.
[29] M. Kobayashi, F. Usui-Kawanishi, T. Karasawa, H. Kimura, S. Watanabe, N. Mise, F. Kayama, T. Kasahara, N. Hasebe, M. Takahashi, The cardiac glycoside ouabain activates NLRP3 inflammasomes and promotes cardiac inflammation and dysfunction, PLoS One 12 (2017), https://doi.org/10.1371/journal.pone.0176676.
[30] S. Lacroix-Lamandé, M.F. d'Andon, E. Michel, G. Ratet, D.J. Philpott, S.E. Girardin, I.G. Boneca, A. Vandewalle, C. Werts, Downregulation of the Na/K-ATPase pump by leptospiral glycolipoprotein activates the NLRP3 inflammasome, J. Immunol. 188 (2012) 2805–2814, https://doi.org/10.4049/jimmunol.1101987.
[31] F. Cornelius, M. Habeck, R. Kanai, C. Toyoshima, S.J.D. Karlish, General and specific lipid-protein interactions in Na,K-ATPase, Biochim. Biophys. Acta 1848 (2015) 1729–1743, https://doi.org/10.1016/j.bbamem.2015.03.012.
[32] A. Christ, P. Günther, M.A.R. Lauterbach, P. Duewell, D. Biswas, K. Pelka, C.J. Scholz, M. Oosting, K. Haendler, K. Baßler, K. Klee, J. Schulte-Schrepping, T. Ulas, S.J.C.F.M. Moorlag, V. Kumar, M.H. Park, L.A.B. Joosten, L.A. Groh, N.P. Riksen, T. Espevik, A. Schlitzer, Y. Li, M.L. Fitzgerald, M.G. Netea, J.L. Schultze, E. Latz, Western diet triggers NLRP3-dependent innate immune reprogramming, Cell. 172 (2018) 162–175.e14, https://doi.org/10.1016/j.cell.2017.12.013.
[33] T. Karasawa, A. Kawashima, F. Usui-Kawanishi, S. Watanabe, H. Kimura, R. Kamata, K. Shirasuna, Y. Koyama, A. Sato-Tomita, T. Matsuzaka, H. Tomoda, S.-Y. Park, N. Shibayama, H. Shimano, T. Kasahara, M. Takahashi, Saturated fatty acids undergo intracellular crystallization and activate the NLRP3 inflammasome in macrophages, Arterioscler. Thromb. Vasc. Biol. 38 (2018) 744–756, https://doi.org/10.1161/ATVBAHA.117.310581.
[34] K. Halbleib, K. Pesek, R. Covino, H.F. Hofbauer, D. Wunnicke, I. Hänelt, G. Hummer, R. Ernst, Activation of the unfolded protein response by lipid bilayer stress, Mol. Cell 67 (2017) 673–684.e8, https://doi.org/10.1016/j.molcel.2017.06.012.
[35] L.A.J. O'Neill, R.J. Kishton, J. Rathmell, A guide to immunometabolism for immunologists, Nat. Rev. Immunol. 16 (2016) 553–565, https://doi.org/10.1038/nri.2016.70.
[36] J.-S. Moon, K. Nakahira, K.-P. Chung, G.M. DeNicola, M.J. Koo, M.A. Pabón, K.T. Rooney, J.-H. Yoon, S.W. Ryter, H. Stout-Delgado, A.M.K. Choi, NOX4-dependent fatty acid oxidation promotes NLRP3 inflammasome activation in macrophages, Nat. Med. 22 (2016) 1002–1012, https://doi.org/10.1038/nm.4153.
[37] D. Namgaladze, S. Lips, T.J. Leiker, R.C. Murphy, K. Ekroos, N. Ferreiros, G. Geisslinger, B. Brüne, Inhibition of macrophage fatty acid β-oxidation exacerbates palmitate-induced inflammatory and endoplasmic reticulum stress responses, Diabetologia. 57 (2014) 1067–1077, https://doi.org/10.1007/s00125-014-3173-4.
[38] E. Rysman, K. Brusselmans, K. Scheys, L. Timmermans, R. Derua, S. Munck, P.P. Van Veldhoven, D. Waltregny, V.W. Daniëls, J. Machiels, F. Vanderhoydonc, K. Smans, E. Waelkens, G. Verhoeven, J.V. Swinnen, De novo lipogenesis protects cancer cells from free radicals and chemotherapeutics by promoting membrane

lipid saturation, Cancer Res. 70 (2010) 8117–8126, https://doi.org/10.1158/0008-5472.CAN-09-3871.
[39] M.A. Gianfrancesco, N. Paquot, J. Piette, S. Legrand-Poels, Lipid bilayer stress in obesity-linked inflammatory and metabolic disorders, Biochem. Pharmacol. (2018), https://doi.org/10.1016/j.bcp.2018.02.022.
[40] H.-J. Kaiser, D. Lingwood, I. Levental, J.L. Sampaio, L. Kalvodova, L. Rajendran, K. Simons, Order of lipid phases in model and plasma membranes, Proc. Natl. Acad. Sci. U. S. A. 106 (2009) 16645–16650, https://doi.org/10.1073/pnas.0908987106.
[41] Y. Li, M. Ge, L. Ciani, G. Kuriakose, E.J. Westover, M. Dura, D.F. Covey, J.H. Freed, F.R. Maxfield, J. Lytton, I. Tabas, Enrichment of endoplasmic reticulum with cholesterol inhibits sarcoplasmic-endoplasmic reticulum calcium ATPase-2b activity in parallel with increased order of membrane lipids: implications for depletion of endoplasmic reticulum calcium stores and apoptosis in cholesterol-loaded macrophages, J. Biol. Chem. 279 (2004) 37030–37039, https://doi.org/10.1074/jbc.M405195200.
[42] M.D. Jensen, Fate of fatty acids at rest and during exercise: regulatory mechanisms, Acta Physiol. Scand. 178 (2003) 385–390, https://doi.org/10.1046/j.1365-201X.2003.01167.x.
[43] M. Habeck, H. Haviv, A. Katz, E. Kapri-Pardes, S. Ayciriex, A. Shevchenko, H. Ogawa, C. Toyoshima, S.J.D. Karlish, Stimulation, inhibition, or stabilization of Na,K-ATPase caused by specific lipid interactions at distinct sites, J. Biol. Chem. 290 (2015) 4829–4842, https://doi.org/10.1074/jbc.M114.611384.
[44] M. Habeck, E. Kapri-Pardes, M. Sharon, S.J.D. Karlish, Specific phospholipid binding to Na,K-ATPase at two distinct sites, Proc. Natl. Acad. Sci. U. S. A. 114 (2017) 2904–2909, https://doi.org/10.1073/pnas.1620799114.
[45] R. Rodrigo, J.P. Bächler, J. Araya, H. Prat, W. Passalacqua, Relationship between (Na + K)-ATPase activity, lipid peroxidation and fatty acid profile in erythrocytes of hypertensive and normotensive subjects, Mol. Cell. Biochem. 303 (2007) 73–81, https://doi.org/10.1007/s11010-007-9457-y.
[46] R. Rodrigo, A. Miranda-Merchak, R. Valenzuela Grau, J.P. Bachler, L. Vergara, Modulation of (Na,K)-ATPase activity by membrane fatty acid composition: therapeutic implications in human hypertension, Clin. Exp. Hypertens. N. Y. N 36 (2014) (1993) 17–26, https://doi.org/10.3109/10641963.2013.783048.
[47] B. Bhatt-Wessel, T.W. Jordan, J.H. Miller, L. Peng, Role of DGAT enzymes in triacylglycerol metabolism, Arch. Biochem. Biophys. 655 (2018) 1–11, https://doi.org/10.1016/j.abb.2018.08.001.
[48] K.M.P. Caldo, J.Z. Acedo, R. Panigrahi, J.C. Vederas, R.J. Weselake, M.J. Lemieux, Diacylglycerol acyltransferase 1 is regulated by its N-terminal domain in response to allosteric effectors1[OPEN], Plant Physiol. 175 (2017) 667–680. doi:https://doi.org/10.1104/pp.17.00934.
[49] S. Kersten, Mechanisms of nutritional and hormonal regulation of lipogenesis, EMBO Rep. 2 (2001) 282–286, https://doi.org/10.1093/embo-reports/kve071.
[50] S.K. Abbott, P.L. Else, T.A. Atkins, A.J. Hulbert, Fatty acid composition of membrane bilayers: importance of diet polyunsaturated fat balance, Biochim. Biophys. Acta BBA - Biomembr. 1818 (2012) 1309–1317, https://doi.org/10.1016/j.bbamem.2012.01.011.
[51] E.K. Lund, L.J. Harvey, S. Ladha, D.C. Clark, I.T. Johnson, Effects of dietary fish oil supplementation on the phospholipid composition and fluidity of cell membranes from human volunteers, Ann. Nutr. Metab. 43 (1999) 290–300.
[52] A. Andersson, C. Nälsén, S. Tengblad, B. Vessby, Fatty acid composition of skeletal muscle reflects dietary fat composition in humans, Am. J. Clin. Nutr. 76 (2002) 1222–1229.
[53] F. Soriguer, S. García-Serrano, J.M. García-Almeida, L. Garrido-Sánchez, J. García-Arnés, F.J. Tinahones, I. Cardona, J. Rivas-Marín, J.L. Gallego-Perales, E. García-Fuentes, Changes in the serum composition of free-fatty acids during an intravenous glucose tolerance test, Obes. Silver Spring Md. 17 (2009) 10–15, https://doi.org/10.1038/oby.2008.475.
[54] M. Pilon, Revisiting the membrane-centric view of diabetes, Lipids Health Dis. 15 (2016), https://doi.org/10.1186/s12944-016-0342-0.
[55] M. Borkman, L.H. Storlien, D.A. Pan, A.B. Jenkins, D.J. Chisholm, L.V. Campbell, The relation between insulin sensitivity and the fatty-acid composition of skeletal-muscle phospholipids, N. Engl. J. Med. 328 (1993) 238–244, https://doi.org/10.1056/NEJM199301283280404.
[56] P.M. Clifton, P.J. Nestel, Relationship between plasma insulin and erythrocyte fatty acid composition, Prostaglandins Leukot. Essent. Fatty Acids. 59 (1998) 191–194.
[57] E. Bakan, A. Yildirim, N. Kurtul, M.F. Polat, H. Dursun, K. Cayir, Effects of type 2 diabetes mellitus on plasma fatty acid composition and cholesterol content of erythrocyte and leukocyte membranes, Acta Diabetol. 43 (2006) 109–113, https://doi.org/10.1007/s00592-007-0224-4.
[58] N.G. Forouhi, A. Koulman, S.J. Sharp, F. Imamura, J. Kröger, M.B. Schulze, F.L. Crowe, J.M. Huerta, M. Guevara, J.W.J. Beulens, G.J. van Woudenbergh, L. Wang, K. Summerhill, J.L. Griffin, E.J.M. Feskens, P. Amiano, H. Boeing, F. Clavel-Chapelon, L. Dartois, G. Fagherazzi, P.W. Franks, C. Gonzalez, M.U. Jakobsen, R. Kaaks, T.J. Key, K.-T. Khaw, T. Kühn, A. Mattiello, P.M. Nilsson, K. Overvad, V. Pala, D. Palli, J.R. Quirós, O. Rolandsson, N. Roswall, C. Sacerdote, M.-J. Sánchez, N. Slimani, A.M.W. Spijkerman, A. Tjonneland, M.-J. Tormo, R. Tumino, D.L. van der A, Y.T. van der Schouw, C. Langenberg, E. Riboli, N.J. Wareham, Differences in the prospective association between individual plasma phospholipid saturated fatty acids and incident type 2 diabetes: the EPIC-InterAct case-cohort study, Lancet Diabetes Endocrinol. 2 (2014) 810–818. doi:https://doi.org/10.1016/S2213-8587(14)70146-9.
[59] J. Kröger, S. Jacobs, E.H.J.M. Jansen, A. Fritsche, H. Boeing, M.B. Schulze, Erythrocyte membrane fatty acid fluidity and risk of type 2 diabetes in the EPIC-Potsdam study, Diabetologia. 58 (2015) 282–289, https://doi.org/10.1007/s00125-014-3421-7.